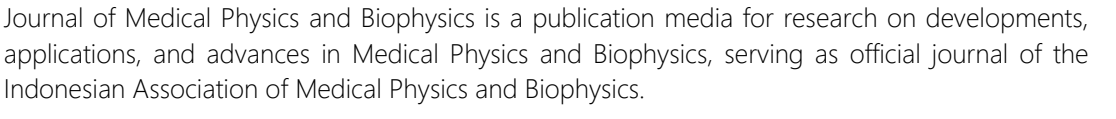
JOURNAL

MEDICAL PHYSICS AND BIOPHYSICS

INAUGURAL ISSUE (VOLUME 1, NUMBER 1) ISSN 2355-2727 FEBRUARY 2014 ONLINE ACCESS: http://jmpb.org 72.82 cGy Film measurements on interventional radiology patients. See more at pp. 21-26









JOURNAL

MEDICAL PHYSICS AND BIOPHYSICS

EDITOR

Chief Supriyanto Ardjo Pawiro, Ph.D

Deputy Yessie Widya Sari, M.Si

BOARD OF REVIEWERS

Chief Djarwani S. Soejoko, Prof. Dr. University of Indonesia

Members Kin Yin Cheung, Ph.D IOMP

Wahyu Setia Budi, Prof. Dr.

H. J. Freisleben, Prof. Dr. rer. med. habil.

Diponegoro University
University of Indonesia

James C. L. Lee, Ph.D NCC Singapore

Musaddiq Musbach, Dr. rer. nat.

University of Indonesia

Hya Kyung Son, Ph.D.

KEDA South Korea

Hye-Kyung Son, Ph.D KFDA South Korea
Johan Noor, Ph.D Brawijaya University

Husin Alatas, Dr.

Idam Arif, Dr.

Bogor Agricultural University
Bandung Institute of Technology

Gede Bayu Suparta, Ph.D Gadjah Mada University

Freddy Haryanto, Dr. rer. nat. Bandung Institute of Technology

TECHNICAL SUPPORT

Journal Manager Lukmanda Evan Lubis (<u>lukmanda.evan@sci.ui.ac.id</u>)
Online Administrator Yakub Aqib Bayhaqi (<u>yakub.aqib@sci.ui.ac.id</u>)

Secretary Ade Rizki Setiadi (ade.rizki@ui.ac.id)

PUBLISHER CONTACT

Email: editor@jmpb.org

Medical Physics and Biophysics Division, Department of Physics, Faculty of Mathematics and Natural

Sciences, University of Indonesia, Depok, 16424, West Java, INDONESIA

Print ISSN: 2355-2727 | Online ISSN: 2355-2719 | http://jmpb.org



JOURNAL

MEDICAL PHYSICS AND BIOPHYSICS

Inaugural Issue (Volume 1, Number 1)

ISSN 2355-2727

February 2014

Online Access: http://jmpb.org

E d i t o r i a l	
JMPB'S INAUGURAL ISSUE JMPB Editor-in-chief	1
Invited Paper	
COMPOSITION OF HUMAN BONE MINERAL BY FTIR AND ITS RELATIONSHIP TO THE AGE	0.7
D. S. Soejoko, Y. W. Sari, S. U. Dewi, Nurizati, K. Dahlan, and D. S. Atmadja	2-7
Inaugural Papers	
OCCUPATIONAL DOSE ESTIMATION WITH FIELD SIZE, POSITION AND C- ARM GANTRY TILT VARIATIONS DURING INTERVENTIONAL CARDIOLOGY PROCEDURES	
N.G. Pratiwi, S.A. Pawiro, K.T. Wigati, D.S. Soejoko	8-13
PERIPHERAL DOSE MEASUREMENT FOR 6 MV PHOTON BEAM N.I. Mohsin, A. Zakaria, R. Abdullah, M.F. Wong	14-15
VOLUME AVERAGING CORRECTION FACTOR OF SEVERAL DETECTORS IN SMALL FIELD RADIOTHERAPY DOSIMETRY F. Haristyo, S.A. Pawiro	16-20
ENTRANCE SKIN DOSE MEASUREMENT USING GAFCHROMIC DOSIMETRY FILM FOR ADULT PATIENTS UNDERGOING CORONARY ANGIOGRAPHY (CA) AND PERCUTANEOUS TRANSLUMINAL CORONARY ANGIOPLASTY (PTCA)	
E. Nurtriningsih, K.T. Wigati, E. Ingrina, Yurneli, S.A. Pawiro	21-26
Guideline Set	
HOW TO PUBLISH IN JOURNAL OF MEDICAL PHYSICS AND BIOPHYSICS: AN	
AUTHOR'S WRITING GUIDELINE A guideline for authors in preparing their manuscripts	i-iii
HOW TO SUBMIT IN JOURNAL OF MEDICAL PHYSICS AND BIOPHYSICS: AN AUTHOR'S TECHNICAL GUIDELINE	
A companion for authors in submitting their manuscripts	iv-vii
HOW TO REVIEW ARTICLES IN JOURNAL OF MEDICAL PHYSICS AND BIOPHYSICS: A REVIEWER'S GUIDELINE	
A guideline for reviewers to conduct reviews on JMPB	viii-ix

JOURNAL OF MEDICAL PHYSICS AND BIOPHYSICS: THE INAUGURAL ISSUE

JMPB Chief Editor

E-mail: editor@jmpb.org

It is a great honor for Medical Physics and Biophysics Division, Department of Physics, Faculty of Mathematics and Natural Science, University of Indonesia, to present the inaugural issue of Journal of Medical Physics and Biophysics (JMPB). In this first issue, a special section entitled 'Inaugural Papers' containing non-reviewed papers that has been orally presented (abstract only) at 8th SEACOMP (Mohsin et al.) and 13th AOCMP (Pratiwi et al) is on the spotlight. A featuring 'Invited Papers' is also presented to display a publication of merit as an opening for the journal. The idea to start a journal dedicated to medical physics and biophysics research and practice for academician, practitioners, and clinical professionals begun in the late 2012. Through numbers of preparation stages and delays, the first issue was set to be published in no later than February 2014. Being endorsed by Indonesian Medical Physics and Biophysics Association as its official publication media, Journal of Medical Physics and Biophysics (JMPB) is currently the first publication to present works in medical physics and biophysics in one journal.

With confidence, it is hoped that the availability of a publication media will enhance the development of medical physics and biophysics researches altogether. We strongly condone that only original works to be submitted in JMPB. Plagiarism, of all, is the most discouraged act.

It is a pleasure to acknowledge the support and encouragement from many sides. Distinguished reviewers, helpers, as well as submitting authors are among the ones we appreciate immensely. Our audience also have a significant role to play in the further development of the journal by disseminating it among their fellow scientists and colleagues, submitting manuscripts for review to be published, and of course by advising us on how the journal can be enhanced.

Supriyanto Ardjo Pawiro, Ph.D *Chief Editor* Journal of Medical Physics and Biophysics

CONGRATULATION MESSAGE FROM THE PRESIDENT OF IOMP

I wish to congratulate the Indonesian Association of Medical Physics and Biophysics (HFMBI) and the Medical Physics and Biophysics Division of Department of Physics, University of Indonesia for successfully launching the Journal of Medical Physics and Biophysics

The journal provides a platform for medical physicists to share their experience, ideas and research findings. It will be a valuable and important source of scientific and professional information for our colleagues practicing in the health industry or research and academic institutions, particularly those in the SEAFOMP and AFOMP regions. Medical physicists are

encouraged to make use of this journal to present their work or to learn from other's work.

I would like to congratulate the Chief Editor, Dr. Supriyanto Ardjo Pawiro and his team for their achievement in launching the journal. I would also like to thank them for their efforts and commitments in running the journal for open access and for their contributions in promoting the advancement of medical physics. I wish the journal every success in achieving its objective and will soon becoming a popular major international research journal.

Kin Yin Cheung, Ph.D

President
International Organization of Medical Physics (IOMP)

COMPOSITION OF HUMAN BONE MINERAL BY FTIR AND ITS RELATIONSHIP TO THE AGE

D. S. Soejoko¹, Y. W. Sari², S. U. Dewi², Nurizati², K. Dahlan², and D. S. Atmadja³

- Department of Physics, Faculty of Mathematics and Sciences, University of Indonesia, Kampus UI Depok 16424, Indonesia
- ² Department of Physics, Faculty of Mathematics and Natural Sciences, Bogor Agricultural University, Jl. Meranti, kampus IPB Darmaga Bogor 16680, Indonesia
- ^{3.} Department of Forensic Medicine and Medicolegal, Faculty of Medicine, University of Indonesia, Jl. Salemba Raya No.6 Jakarta Pusat 10430, Indonesia

E-mail: djarwani@fisika.ui.ac.id

Abstract: Deproteinated human bone with hydrazine indicated that percentage of bone mass mineral increased with individual age in the range of child to adult, and then slowly decreased with ageing. Type of bone and sex also influenced the proportional of mineral in bone. Several information was obtained from infrared spectroscopy measurements. Calcium phosphate in bone mineral was a mixture of amorphous calcium phosphates and apatite crystals that rich of carbonates. Most crystals were carbonate apatite type B, with additional small amount of type A and AB. The splitting factor of v4 phosphate bands indicated that crystalline degree was regulated by age, increases in the range of child to adult, then decrease up to a certain value (0.16) and finally almost constant. It is predicted that apatite crystals that was formed with less calcium phosphate will accompanied by the insertion of crystallization water in order to maintain the constancy of bone volume.

Received 2 October 2013 Published 30 December 2013

Keywords: human bone mineral, apatite crystal, water crystallization

I. INTRODUCTION

Although Glimcher et al (1981) argued the presence of amorphous phase during bone formation, current study conducted by (Olszta et al., 2007) supported previous observation of Termine and Posner (1966 and 1967) in which they called up the idea of both amorphous and crystalline phase were presence in bone mineral. Infrared spectroscopy indicated that besides phosphate, carbonate is also present in bone mineral which is incorporates with either amorphous or crystalline calcium phosphate. However, the existence of carbonate in an amorphous environment is still indeterminate. On the other hand, in calcium phosphate of bone mineral known as apatite crystal of which its structure is analogous to stoichiometric hydroxyapatite, Ca₁₀(PO₄)₆(OH)₂, carbonate ions may replace either OH or PO₄3- ion and are designated as carbonate apatite type A and type B respectively. Two sets of infrared absorption bands at about 1545, 1450, 880 cm⁻¹, and 1465, 1412, 872 cm⁻¹ correspond to carbonate apatite type A and type B (Termine and Lundy, 1973). In addition, there is also exist an unstable carbonate apatite which is introduced as type AB and characterized by the bands at 1452 - 1470 -1500 - 1545 - 1568 cm⁻¹ (Rey et al., 1989, 1991).

In this paper, infrared spectroscopy of human bone mineral with differ individual age is reported. Obtaining the information of bone mass percentage, hydrazine was used to remove organic component from bone samples that most of

The *Invited Paper* section in *Journal of Medical Physics and Biophysics* serves in publishing selected works with merit. No review process was applied unto the works published in the section.

which were taken from rib. Further investigation was carried out by Fourier Transform Infrared spectrometer (FTIR).

II. MATERIALS AND METHODS

Ten human bone samples were obtained from ten individuals who came to autopsy. It is believed that the subjects were in normal health prior to passed away. Those samples represented the age groups of child (1 day), adolescence (16 years), adult (21 - 36 years), and old (60-75)years. Most samples were selected from rib, and others were from femur, head, and tibia. First all samples were deproteinated to separate bone minerals from its organic compounds. Hydrazine was preferred than ethylenediamine and hyphochlorite for deproteination as hydrazine did not alter the mineral phase in the treated sample (Termine, Eanes, Greensfield, Nylon, 1973 and Tomazic, Brown, Eanes, 1993). Samples were immersed into 10 ml of hydrazinium hydroxide for 1 hour at ambient temperature. Reimmersion was done subsequently for 2 hours at room temperature, 1 hour at 60 °C, and 24 hours at 60 °C. Then samples were diplo washed using 50, 75, 85, and 100 % ethanol and followed by aquadest. To remove adsorbed water, samples were heated at 110 °C for 12 hours.

For infrared spectroscopy measurement a milligram of sample was mixed with about 100 mg KBr, grounded and pressed in the mould to produce transparent pellet. All infrared spectra were obtained using Brucker FTIR spectrometer, with the measurement range of $400-400~{\rm cm}^{-1}$. Wave numbers where transmission peaks occurred were recorded at each spectrum.

III. RESULTS AND DISCUSSION

Mass of bone minerals of 10 samples that was obtained from deproteination using hydrazinium hydroxide is presented in Table 1. These samples were originated from the rib (7 samples), the femur (1 sample), the head (1 sample), and the tibia (1 sample). Most samples were obtained from different individual and at different age, except 1 rib and 1 head samples were taken from the same male person at the age of 31 years. From these two samples, it is shown that the head has higher content of mineral mass than that of the rib. Figure 1 illustrates the relation between the bone mineral mass with the individual age. The mass percentage value for an individual age between 16 to 75 years is in the range of 20 -50 % with the tendency to decrease with the ripening.

Table 1 Mass of human bone minerals originated from various age of individual.

Category	Sex	Age	Type	Mass (% wt)
Child	Male	1 day	Femur	42,33
Adolescence	Male	16 years	Rib	50,65
Adult	Male	30 years	Rib	32,99
		31 years	Rib	48,12
		31 years	Head	65,05
		36 years	Tibia	56,27
Adult	Female	21 years	Rib	43,03
Old	Male	60 years	Rib	34,24
		65 years	Rib	25,47
Old	Female	75 years	Rib	23,85

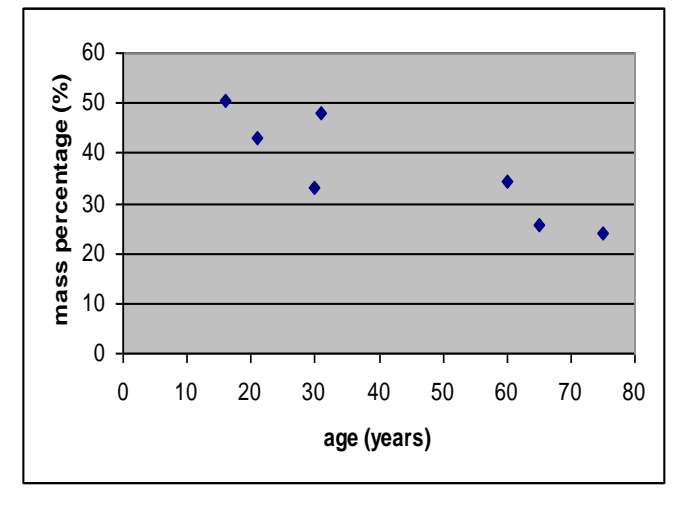


Figure 1. Percentage mass human bone minerals of the rib in relation with individual age.

The result of FTIR spectroscopy is illustrated in Figure 3. Band positions of recorded spectra are presented in Table 3. Of all appeared phosphate bands, there are two bands that occur in all spectra, the $\nu 3$ band in the range of 1000-1200 cm-1 and the $\nu 4$ band in the range of 500-700 cm-1. The $\nu 3$ band is a broad and asymmetry band with the peak at about 1032-1037. While the $\nu 4$ band is split into two peaks at 605 and 566 cm-1 which indicate that the sample contains apatite crystals. Besides these two phosphate bands, there is also $\nu 1$ phosphate band at about 962 cm-1 as a shoulder of the $\nu 3$ band.

The carbonate bands present at lower intensity compare to that of the phosphate bands. The υ_3 carbonate band is located at $1400-1600~\text{cm}^{-1}$, and the υ_2 band is at about 873 cm⁻¹. All spectra contain υ_3 carbonate broad band with two peaks at about 1418 and 1453 cm⁻¹. Some spectra also exhibit additional small band with peaks at about 1542 and 1560 cm⁻¹. A Sharp υ_2 carbonate band can be seen clearly at about 873 cm⁻¹ in all spectra. The bands at about 1545, 1450, and 880 cm⁻¹ are attributed to carbonate apatite type A, and the bands at about 1465, 1412, and 872 are recognized as carbonate apatite type B (Termine and Lundy, 1973). The broad band with peaks at about 1418, 1453, 1542, and 1560 cm⁻¹ is match with character most bands of type AB carbonate apatite (Rey et al. , 1989, 1991).

The splitting of the v4 phosphate band can be used for estimating the crystallization degree in mixtures of amorphous calcium phosphate and apatite crystal (Termine and Posner, Science, 1966). Evaluating the crystalline degree quantitatively, the splitting factor (SF) is defined as the ratio between AB and AC (Figure 2). The SF value of all samples is presented in Table 3. It can be noticed that SF is initially influenced by age on which its value is increase significantly from 0.18 (a born child /1 day) up to 0.25 (an adolescence/16 years), and then followed by a decline to 0.16 (adult/31 years). Afterwards, its value is relatively constant up to the age of 65 years. If SF at a born child (0.18) is assumed as a reference, at adolescence its value increases approximately up to 39% and at the age between adult and old its value increases only about 11 %. SF value as a function of age is presented in Fig. 4.

The existence of adsorbed water in all samples is indicated by the broad band at $3700-2500~\rm cm^{-1}$. Several sharp peaks that appear between $3300-1600~\rm cm^{-1}$ are recognized as water of crystallization. Along this region, there are at least three distinct peaks, one peak in the region of $1600-1650~\rm cm^{-1}$ and the two others in $2850-2930~\rm cm^{-1}$.

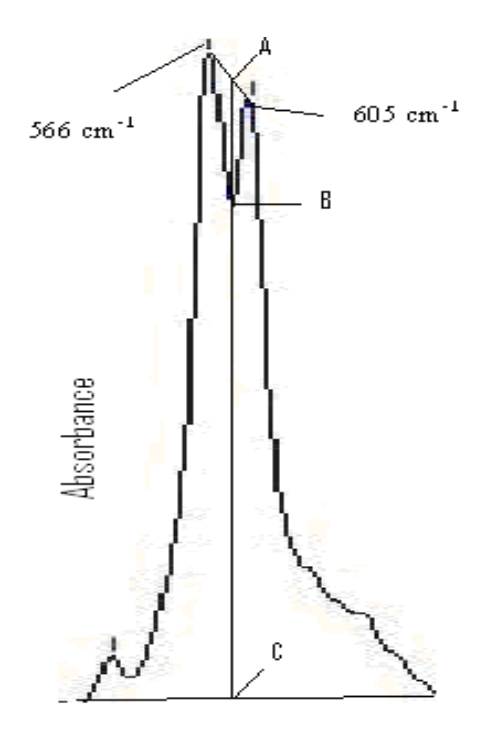


Figure 2. Illustration of splitting factor (SF= AB/AC) of v_4 phosphate band.

Soejoko, et al.

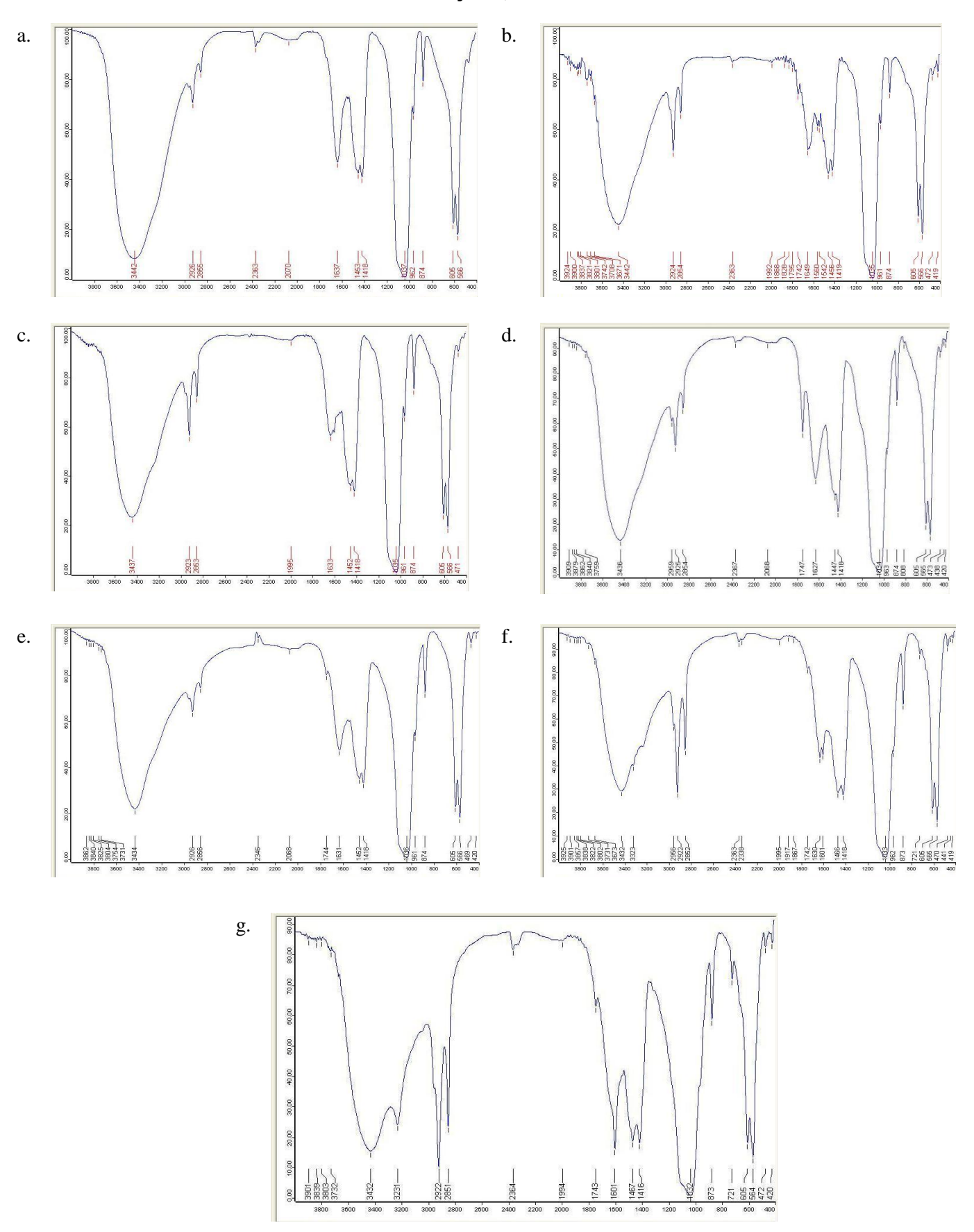


Figure 3. Infrared spectra human bone minerals of individual with the age of a) 1 day, b) 16 years, c)30 years, d) 31 years, e) 36 years, f) 60 years, and g) 65 years.

Soejoko, et al.

Table 2. Position of absorbed bands for phosphates, carbonates, and water crystals in infrared spectra of human bone minerals.

A	Т		Phosphate (ci	n -1)		Carbonate (cm ⁻¹	4)	Crystalliza	tion water
Age	Type	v_1	v_3	v_4	Y_2	v_3	v_4		
1			_	605		1453	_		2926
day	Femur	962	1037	566	566 872	1418	-	1637	2866
				605		1419			2924
16	Rib	061	1035		1456		1649		
yrs	KIU	961	1055	566	874	1542		1049	2854
						1560			
30				605		1452	_		2923
yrs	Rib	961	1035	566	566 874	1418	-	1633	2863
21				605		1447		1627	2925
31	Rib 90	963	1034	566	874	1418		1747	2864
yrs				300		1418		1/4/	2959
36	Tibiae	961	1036 -	605	- 874 -	1452	_	1631	2925
yrs	Tiblae	901	1030	566	0/4	1418	-	1744	2856
60			_	605	_	1457	_	1630	2922
yrs	Rib	962	1033	565	873	1417	721	1601	2852
y13			1559	1559			2632		
65		6051457	1457		1601	2922			
yrs	Rib	ib - 1032	564	873	1416	721	1743	<u>2851</u> 3231	
J13	5 304		1416		1/45 —				

Table 3. Splitting factors of the v4 phosphate bands in infrared spectra of human bone mineral.

Age	AB (cm)	AC (cm)	SF
1 day	0.90	4.9	0.18
16 years	1.1	4.4	0.25
30 years	0.95	4.4	0.22
31 years	0.70	4.5	0.16
36 years	0.70	4.5	0.16
60 years	0.75	4.7	0.16
65 years	0.70	4.6	0.15

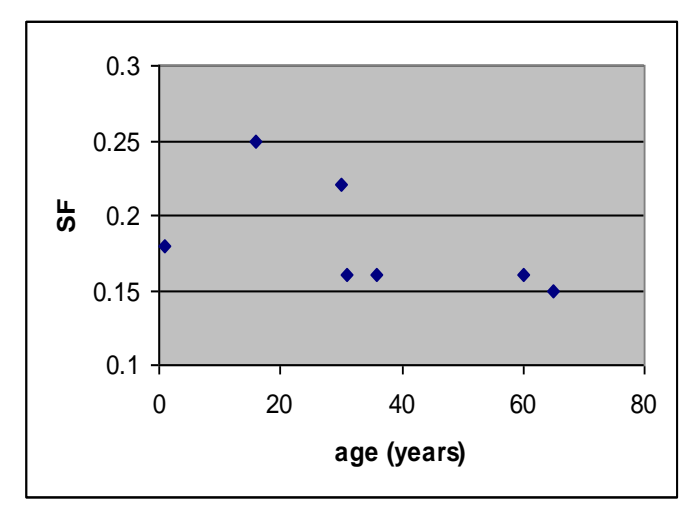


Figure 4. Splitting factor in related with individual age.

As part of biological system, bone mineral is in a relation with metabolic activity. Bone mineral is being continuously deposited and resorbed. Parallel with slowing down of metabolic activity, the bone mineral content also declines with increasing of individual age. This tend can be seen noticeably

from the rib samples (Table 1) of which the percentage bone mineral of an individual from adult (16 years) up to old (65 years) is decrease from 50.65% up to 25.47%. This found support the statement that bone mass of long bone is reduced as much as 60% for women and 50% for men during ageing (Larry L. Hench and Julian R. Jones, 2005). Type of bone is also influenced the proportion of mineral in bone. Compared to the rib, both the head and tibia bones have a higher mass percentage. This relates with their structure. On one site, the head bone is a flat bone completely composed of compact bone. A tibia is a long bone that has two regions, diaphyses and epiphyses. Diaphysses is constructed by compact bone while epiphyses, as an extremity of long bone consist of spongy bone. On another site, rib is constructed by two layers, a compact bone in the outer and a spongy bone in the inner site.

The most stable calcium phosphate is hydroxiapatite (HAP) crystal, $Ca_{10}(PO_4)_6(OH)_2$. Both complex and simple ions in the vicinity of calcium and phosphate ions able to produce biological apatite in bone mineral in similar structure with HAP, but diverse in composition and stoichiometry. The formula of biological apatite can be written as follows

$$(Ca, M)_{10} (PO_4, Y)_6 (OH_2, X)$$

with M represents simple ion such as Mg, Na, and K, and Y represents complex ions such as carbonate and sulphate, whereas X represents either complex or simple ion such as carbonat, fluor, and chlor.

Infrared spectra of bone mineral indicates that most crystal apatite is carbonate apatite type B and some amount of type A, with addition of type AB. Type A and B carbonate apatite is produced by substitution of OH⁻ and PO₄³⁻ with CO₃²⁻ ion, respectively,. While type AB carbonate apatite is not a simple addition of both type A and B but it is predicted that it has a correlation with a poorly crystalline phase (Rey et al., 1989). The presence of carbonate type B is obvious; it is

indicated by the appearance of a strong band at about 873 cm⁻¹. Contrary, the presence of carbonate apatite type A is an ambiguous as there is a disappearance of the peak at 880 cm⁻¹ which is one of its characteristics band. Nevertheless, the absence of OH⁻ bands at about 3572 and 630 cm⁻¹ as characteristic bands of hydroxyl in hydroxyapatite indicates that there is a carbonate substitution to hydroxyl group in hydroxyapatite which result a carbonate type A. The appearance of carbonate type AB is clearly seen in samples with the age of 16 and 60 years.

Apatite crystal in bone mineral includes in metabolism activity. New apatite crystals are always formed, the existed young crystals growth to mature, and the mature crystals come to old. Naturally, the resorption will occur among the oldest, the same trend is also happen in apatite crystal. Therefore bone mineral always contain of apatite crystals with different ages. Using SF of the v4 phosphate band, it can be inferred that crystalline degree of bone mineral is a function of time from the new born up to adolescence. This parameter further decrease up to a certain degree and then inclines up to a constant value during adult to old period. Compare to bone mass percentage, this study suggest that there is no correlation between bone mass percentage and crystalline degree. As an example, though both bone mass percentage from the rib of 30 and 60 year old person has a nearly value (32.99 and 34.24 %, respectively), there is a difference in crystalline degree which is indicated by a varied SF value (0.22 and 0.16, respectively).

All infrared spectra indicated the existence of crystallization water by appearing OH- bands in the range of $1601 - 1747 \text{ cm}^{-1}$ and in the range of $2922 - 3231 \text{ cm}^{-1}$ that further will be called the first and second range. One sharp band at the peak at about 1630 cm⁻¹ always appears clearly in the first range, and two sharp bands with the peaks at about 2860 and 2925 cm⁻¹ are well observable in the second range. The band at 2925 cm⁻¹ is in higher intensity compare with the band at 2860 cm⁻¹. There are other bands with low intensity which are located between the two ranges. All of these bands indicated that more than one type of water environment exist in the crystals. It is interesting to note that intensity of the band in the first range is much higher than those in the second range at the spectra from femur of a new born child (1 day) and tibia of an adult (36 years). A slight different is found at the rib spectra; the bands in the first and second range are comparable in intensity particularly which come from adult (16, 30, and 31 years). A great different appeared at the rib spectra from old individual (60 and 65 years), the bands in first and second range are at high intensity, and moreover those from 65 years person are relatively higher. This is an indication that bone mineral from old individual contains high concentration of crystallization water.

It seems that there is a tendency in which high crystalline degree or high SF value will be accompanied by low degree of water crystallization, vice-versa. These phenomena can be understood since the insertion of water molecules into the crystal lattice will influence the packing arrangement. Metabolism rate of an old individual is relatively lower compare with that happen in young individual, therefore the formation and growth of crystals in bone mineral is not balanced with the body's resorption of calcium from bone. To keep a constant volume of the bone, water molecules might enter crystal lattice and form a hydrogen bond to substitute the crystal destruction.

IV. CONCLUSION

Human bone mineral relates with metabolism activity, and the mass tends to decrease with ageing. From the male rib bone samples, the changes is clearly appeared, in the interval between 16-65 years (adolescence to old individual) the bone mass was found 50.65% and 25.47%. The decrease is started at about individual age of 60 years. Even with limited samples it can also be seen that the percentage bone mass is also influenced by type of bole and sex of individual.

From infrared spectra it is shown that composition of amorphous calcium phosphates and apatite crystals in human bone is also affected by metabolism activity. Most apatites were type B with additional small amount type A and AB. The splitting factor of υ_4 phosphate bands illustrated the crystalline degree of bone mineral. From the rib samples SF decrease from 0.25 to 0.16 that was found at the range of age from 16 to 31 years of individual age. After 31 years of age, the SF value was relatively constant. At any instant bone mineral contains newly formed apatite crystals, young and mature crystals. It was predicted that for maintaining bone volume, crystallization water play a significant role. Apatite crystals which were formed with less of calcium phosphates will be rich of crystallization water in order to maintain the constancy of bone volume.

V. ACKNOWLEDGMENTS

We thanks to dr. Swasti Hertian, Sp.F (The Head of Department), Department of Forensic Medicine and Medicolegal, Faculty of Medicine, University of Indonesia, Jakarta, for the permission to get the human bone sample from autopsy material, and to dr. Evi Untoro for helping us in collecting the human bone sample from autopsy material.

REFERENCES

- [1] Termine J. D. and Lundy D. R., Hydroxide and carbonate in rat bone mineral and its synthetic analogues, Calc. Tiss. Res. 13, 73-82, 1973
- [2] Rey C., Collins B., Goehl T., Dickson I. R., and Glimcher M. J., The carbonate environment in bone mineral: A Resolution enhanced Fourier Transform Infrared Spectroscopy Study, Calc. Tiss. Int. 45, 157-164, 1989.
- [3] Termine J. D., Posner A. S., Infrared analysis of rat bone: Age dependency of amorphous and crystalline mineral fractions, Science 153, 1523-1525, 1966.
- [4] Termine J. D., Posner A. S., Amorphous/crystalline interrelationships in bone mineral, Calc. Tiss., Res., 1, 8-23, 1967.
- [5] Termine J. D., Eanes E. D., Greensfield D. J., and Nylon M. U., Hydrazine deproteinated bone mineral, Calc. Tiss. Res., 12, 73-90, 1973.
- [6] Hench L. L., The skeletal system, in *Biomaterials, artificials organs and tissue engineering* (L. L. Hench and J. R. Jones, Editors), Woodhead Publishing Limited, Cambridge, 2005.
- [7] M.J. Glimcher, L.C. Bonar, M.D. Grynpas, W.J. Landis, A.H. Roufosse, Recent Studies of bone mineral- is the amorphous calcium phosphate theory valid, J. Cryst. Growth 53 (1981) 100-119.

Soejoko, et al.

- [8] Olszta M.J, et al, Bone Structure and Formation: A new perspective, Materials Science and Engineering R 58 (2007) 77-116.
- [9] Rey C, V. Renugopalakrishan, M. Shimizu, B. Collins, and M.J. Glimcher. A resolution-enhanced Fourier Transform Infrared Spectroscopic Study of the environment of the CO32- ion in the
- mineral phase of enamel during its formation and maturation. Calcif Tissue Int (1991) 49: 259-268.
- [10] Tomazic BB. Brown WE, Eanes ED (1993) A Critical evaluation of the purification of biominerals by hyphochlorite treatment. J Biomed Mater Res 27: 217-225

OCCUPATIONAL DOSE ESTIMATION WITH FIELD SIZE, POSITION AND CARM GANTRY TILT VARIATIONS DURING INTERVENTIONAL CARDIOLOGY PROCEDURES

N.G. Pratiwi, S.A. Pawiro, K.T. Wigati, D.S. Soejoko

Medical Physics and Biophysics Division, Department of Physics, Faculty of Mathematics and Natural Sciences, University of Indonesia, Depok, 16424

E-mail: n.gitapratiwi@gmail.com

Abstract: In Interventional Cardiology, dose received by the patient is relatively higher, while the occupational would receive scattered radiation dose whose quality is relatively lower. However, the occupational received accumulative doses of all cardiovascular procedures were done over the years. Therefore, the purpose of this paper will focus to estimate the distribution of scattered dose to occupational without any protective shielding in the Cath Lab. The scattered dose rate was measured by using survey detector of Unfors Xi. The detector was placed at 6 different positions around the phantom. Each measurement position has eleven points from 25 to 175 cm above the floor with increment of 15 cm as the illustration of partial height of occupational organ. Experimentally a Rando phantom was irradiated by automatic pulsed fluoroscopy with condition varies in the range of 88-93 kV and 5.7-9.4 mA depend on gantry tilt and field size. The Philips C-arm gantry tilt was varied at 0° PA projection, 20° and 30° Caudal, 20° and 30° Cranial, and 40° and 50° Left Anterior Oblique, and also Flat Panel Detector (FPD) was varied at 20 x 20 and 25 x 25 cm². Generally, the greatest dose rate was known at level corresponding to the waist (100 cm) of occupational and the lowest at head areas (175 cm) of occupational which is 2.49 mGv/h and 0.02 mGy/h, respectively. The given data showed that the scattered fractions are in the range of 0.001-0.060% from its primary dose at isocenter. The scattered doses tend to increase with gantry tilt for all positions. Increasing field size of FPD will decreased the scattered fraction from its dose at isocenter, and also it affects the scattered dose

Received 15 January 2014 Revised 03 February 2014 Accepted 10 February 2014 Published 28 February 2014

Keywords: Interventional Cardiology, Occupational Dosimetry, Radiation Protection, Scattered Dose Rate

I. INTRODUCTION

involves Interventional cardiology fluoroscopy diagnostic which requires a long time with a low radiation intensity to guide the catheter, and cine radiography which requires a short time with high radiation intensity for documentation of actions. The numbers of percutaneous interventional procedures using radiation have continually increased since the 1960s [1]. In general, both workers and patients in interventional cardiology procedure room are exposed to ionizing radiation. Personnel should be aware of 3 different types of ionizing radiation exposure: the primary xray beam, scattered x-rays, and leakage x-rays. The radiation dose received by the patient is relatively higher because patients are in the primary beam, while the workers would receive scattered radiation dose whose quality is relatively lower and spread in every direction. However, different from the patients, the clinical workers received a cumulative dose of all cardiovascular measures were done over the years. Scattered radiation levels in the room are in the range 0.2 -4.5 mSv/h during the procedure [2].

Based on the ICRP recommendations No. 60 (1990), The maximum annual dose allowed for radiation workers is 20 mSv averaged over 5 years, with no more than 50 mSv in a year. For the lens of the eye it is 150 mSv per year and 500 mSv for the skin, hands, and feet. Therefore, the occupational should be more vigilant at position that has a high scattered radiation. The discussion of the dose distribution in

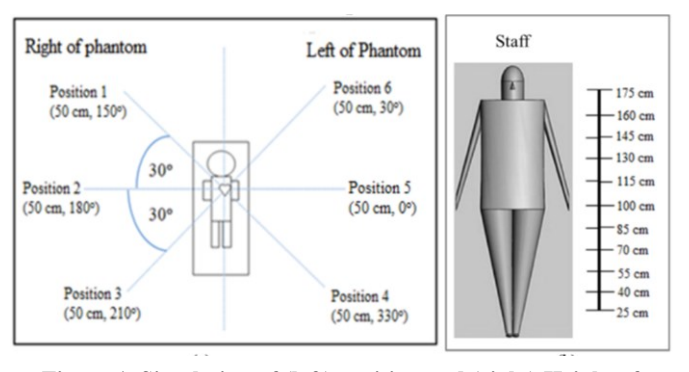


Figure 1. Simulation of (left) position and (right) Height of occupational

interventional cardiology procedures to determine the scattered radiation is very important.

II. MATERIALS AND METHODS

Rando phantom which is assumed as the body of the patient, is placed on the patient table to be irradiated with the radiation field wide 25 cm x 25 cm. Furthermore, the scattered dose rate was observed at six different positions around the patient, as in Figure 1 (left), using Unfors-Xi survey detector. Occupational position is set at a distance of 50 cm away from isocenter. Each measurement position has

eleven points from 25 to 175 cm above the floor with increment of 15 cm as the illustration of partial height of occupational. The gantry tilt was varied at 0° PA projection, 20° and 30° caudal , 20° and 30° cranial, 40° and 50° LAO. The measurement was performed with the patient table height and SID (Source to Intensifier Distance) 102 cm and 100 cm, respectively.

Table 1. Dose rate at isocenter for different angles and FPD based on kV and mAs

FPD (cm ²)	Gantry Tilt	kV	mA	Time (s)	Dose Rate (mGy/s)
20 x 20	0	93	9.4	180	1.170
25 x 25	0	89	6.2	180	1.062
25 x 25	20 CAU	91	6.8	180	1.217
25 x 25	30 CAU	93	7.7	180	1.440
25 x 25	20 CRA	88	5.8	180	0.971
25 x 25	30 CRA	89	6.0	180	1.027
25 x 25	40 LAO	88	5.7	180	0.954
25 x 25	50 LAO	88	5.9	180	0.988

The results will be showed as a percentage where the scattered dose rate is divided by the value of the primary dose rate at isocenter and is multiplied by 100%. This result represents the number of relative scattered doses from its primary beam.

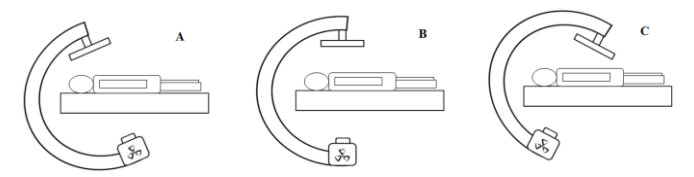


Figure 2. Simulation of gantry tilt of (a) cranial, (b) 0° PA Projection and (c) caudal

III. RESULTS AND DISCUSSION

In this study, the measurement result of air dose rate at the primary beam with a distance of 98 cm from the X-ray tube is obtained as in Table 1. To find out the air dose rate at the isocenter, which is at a distance of 50 cm from the X-ray tube, is using inverse square law formula. Thus, the value of the air dose rate at isocenter is $17.43 \, \mu Gy/s$.

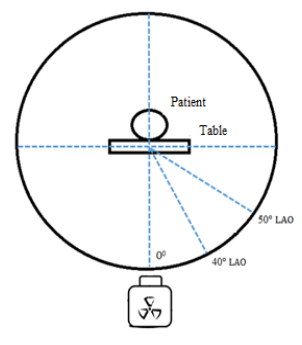


Figure 3. Simulation of gantry tilt of LAO

The Philips C-arm is used specifically for interventional, therefore being not equipped with kV and mAs settings, so the value of the dose rate at the isocenter point should be adjusted as at the time of measurement, using the following Equation 1, where $\dot{D} = \text{absorbed dose rate}$, kV = energy in kilovoltage, mA = current in milliamps, and s = time in second. The air dose rate at isocenter at the time of measurement is showed in Table 2.

$$\dot{D}_2 = \left(\frac{kV_2}{kV_1}\right)^2 \times \left(\frac{mAs_2}{mAs_1}\right) \times \dot{D}_1 \tag{1}$$

Tabel 2. Air dose rate at a distance of 98 cm from the X-ray tube

FPD (cm ²)	kV	mA	Time (s)	μGy/s
20x20	71	4.7	6	2.959
25x25	74	4.7	6	4.537

Generally, the distribution of scattered radiation from a height of 25 cm to 175 cm follows a Gaussian distribution. This scattered results is obtained without any protective shielding in place. Scattering distribution lowest value was found in the head of the occupational (175 cm from the floor). Percentage scattering of these area of the occupational has been hindered by the patient table and the phantom. Additionally, the foot of the occupational (25 cm from the floor) also get scattered radiation with relatively small value because the area is under the x-ray tube collimator. Meanwhile, the largest value obtained in areas with height 85 cm and 100 cm from the floor. The highest value obtained for the scattering of radiation that accumulates on the patient was at table height (102 cm from the floor); at that height, additional backscatter of the patient table and the floor exists.

A. Field Size Variation

For FPD variation, the scattering fraction increased with the decrease of field size for all positions and heights. This is due to the interaction of radiation (photons) with materials that will happen less in the smaller FPD. So the smaller FPD has a scattering that is greater than larger FPD. In addition, the small size of the selected FoV will increase the value of kV on ABC (Auto Brightness Control) fluoroscopy, thereby increasing the radiation dose. This can be seen in Figure 4 through Figure 9, that the FPD 20 x 20 cm² has a scattering fraction that is greater than FPD 25 x 25 cm². In other words, the scattered dose rate received by occupational would be higher on the use of small FPD. It can also be observed that scatter faction for greater heights (130 to 175 cm from the floor) has a smaller values, especially at the height of 175 cm, where the scattering fraction for both FPD matches. It might happen because at the table height radiation has been scattered by the patient, or very little radiation penetrates through, so that this area tends to be safe.

B. Gantry Tilt Variation

When the gantry tilt of 30° and 40° CAU was applied, scattering distribution on the right and left phantom positions

were not symmetrical. Position 1, 2, and 3 simultaneously has a maximum value at 100 cm height, then decrease at a height of 85 cm. While the position 4, 5, and 6 has maximum value at the height of 85 cm. Percentage distribution of scattering radiation was increased with the gantry tilt of caudal (Figures 10-15). This applies to positions 1, 2, 5 and 6. As for the position 3 and 4, the greatest percentage scattering is actually obtained for gantry tilt of 20 CAU, because positions 3 and 4 are on the caudal phantom and far from the x-ray tube.

C. Cranial Gantry Tilt Variation

For variation of cranial gantry tilt, the percentages scattering at positions 2, 3, 4, and 5 increased in line with increasing gantry tilt (as seen on Figures 16-21). However, at positions 1 and 6, on the contrary, the percentage scattering decreased with gantry tilt increase. This is because the x-ray tube is further away from the position of the 1 and 2.

D. LAO Gantry Tilt Variation

Position 4 which has a lower radiation scattering is typically safer than position 3 for the gantry tilt of 40° and 50° LAO. This is because position 3 is very close to x-ray tube, while position 4 received scattering that has been hindered by the patient table. Thus, position 3 tends to get more backscattered radiation. In the Figure 4, position 3 explains that the smaller the gantry tilt of LAO, the smaller percentage value of scattering radiation was obtained. Inversely proportional to the position 4, i.e. in Figure 5, the value of the percentage distribution of the scattering was greater for small gantry tilt. The value of which is inversely proportional to the position 3 and 4 is due to the position 4 being at a position close to the x-ray tube.

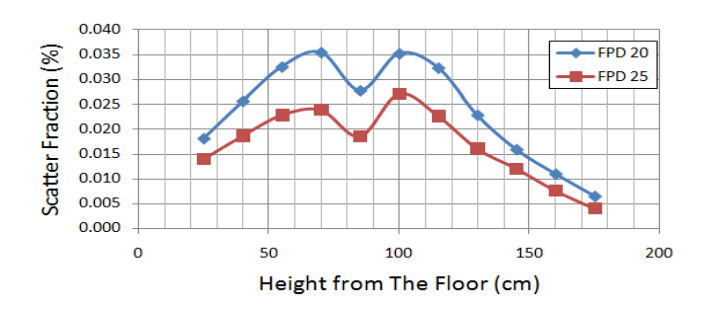


Figure 4. Graph of scattered fraction vs. the height from the floor at position 1 of field size variation

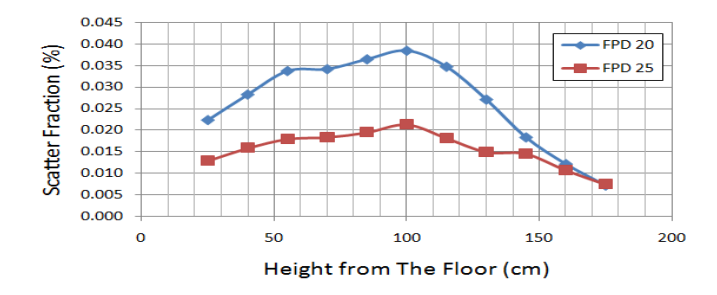


Figure 5. Graph of scattered fraction vs. the height from the floor at position 2 of field size variation

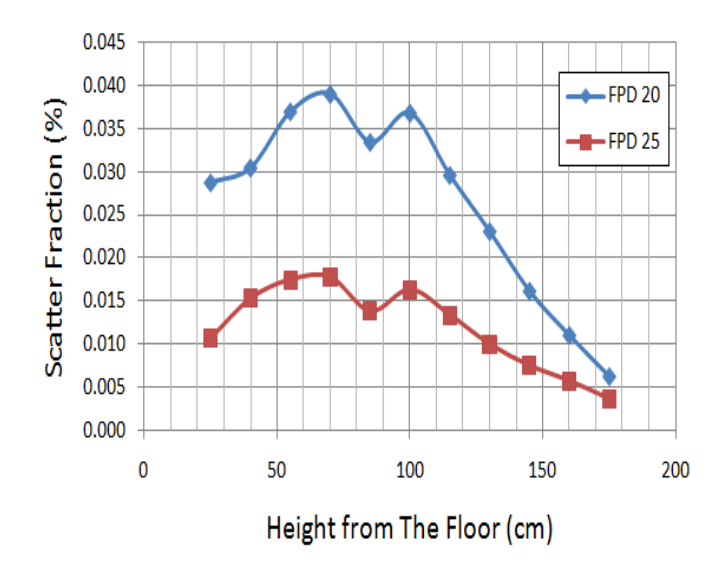


Figure 6. Graph of scattered fraction vs. the height from the floor at position 3 of field size variation

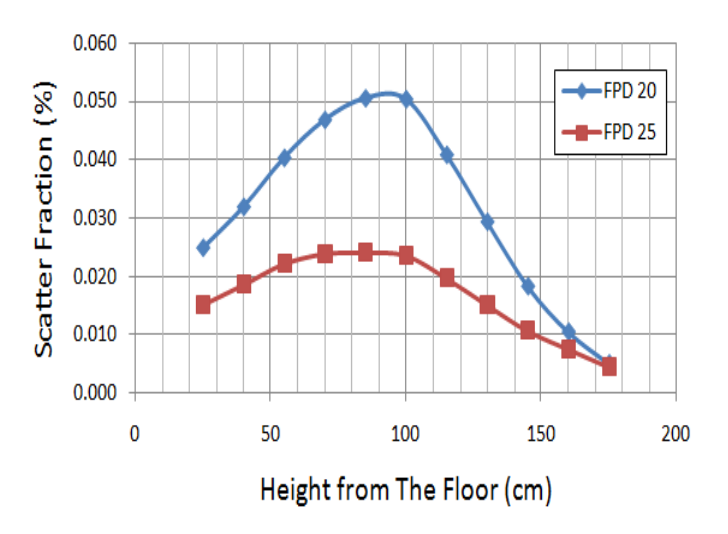


Figure 7. Graph of scattered fraction vs. the height from the floor at position 4 of field size variation

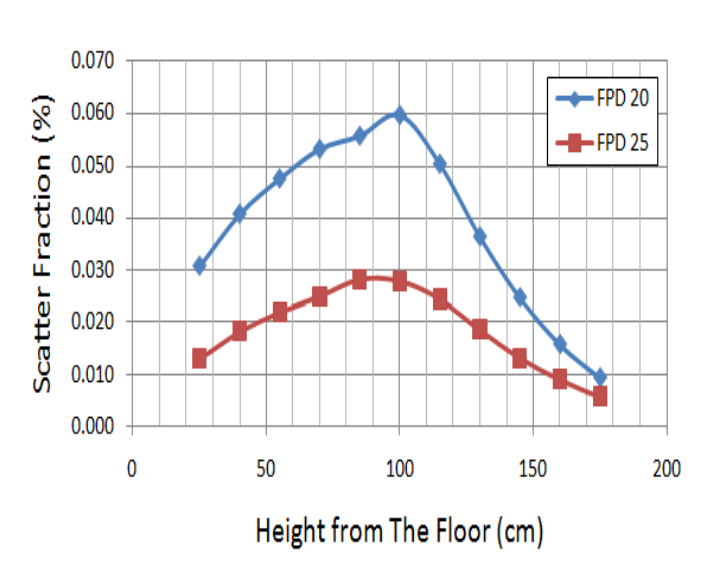


Figure 8. Graph of scattered fraction vs. the height from the floor at position 5 of field size variation

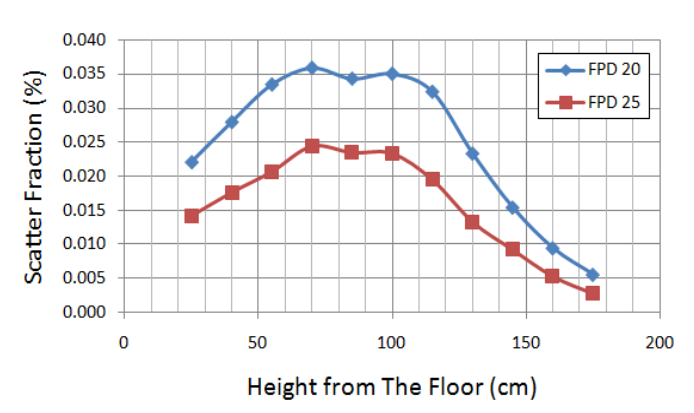


Figure 9. Graph of scattered fraction vs. the height from the floor at position 6 of field size variation

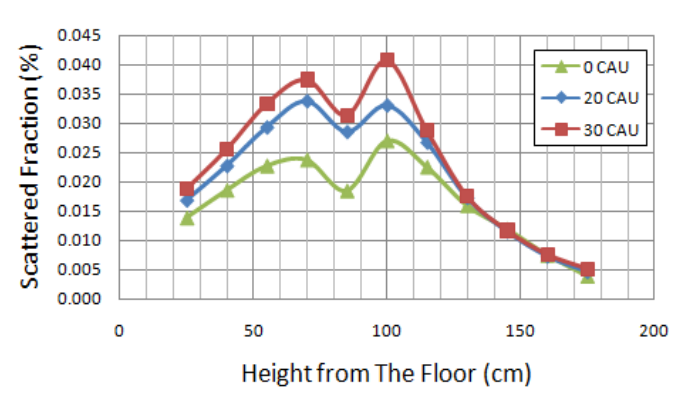


Figure 10. Graph of scattered fraction vs. the height from the floor at position 1 of caudal gantry tilt variation

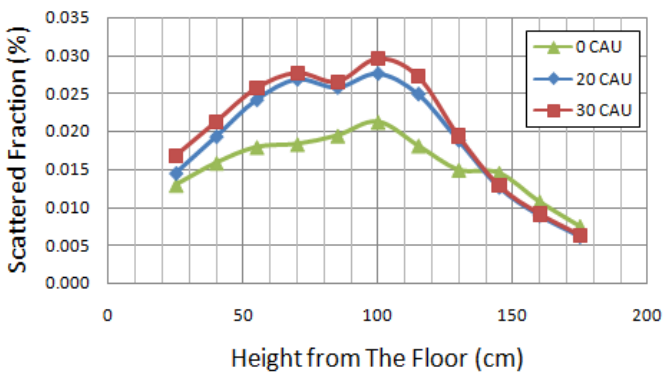


Figure 11. Graph of scattered fraction vs. the height from the floor at position 2 of caudal gantry tilt variation

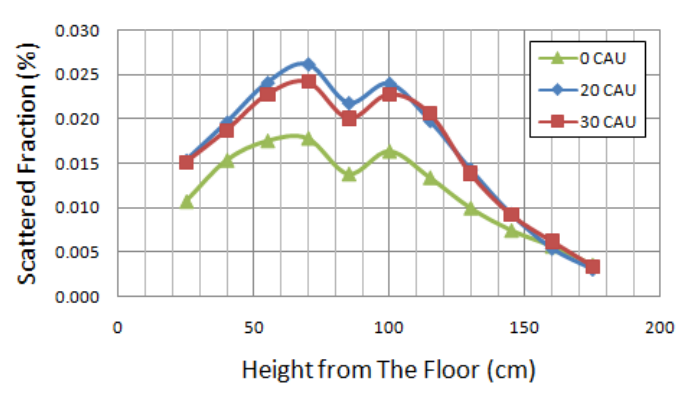


Figure 12. Graph of scattered fraction vs. the height from the floor at position 3 of caudal gantry tilt variation

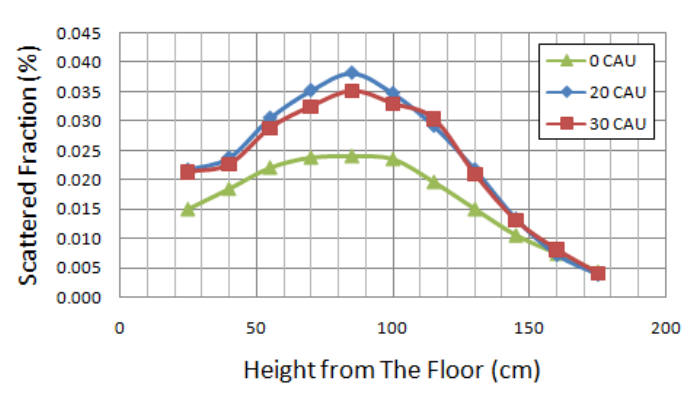


Figure 13. Graph scattered fraction vs. the height from the floor at position 4 of caudal gantry tilt variation

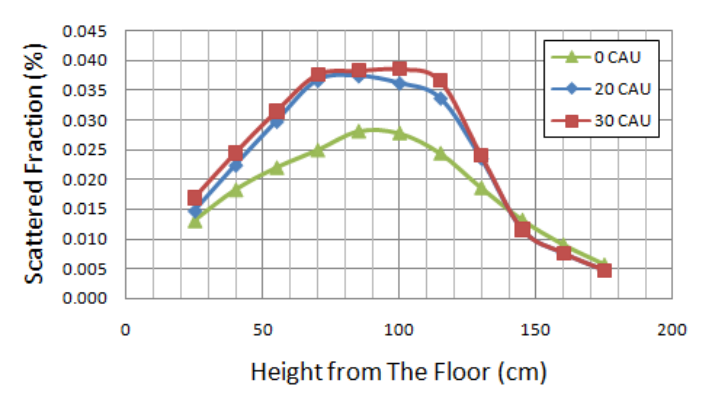


Figure 14. Graph of scattered fraction vs. the height from the floor at position 5 of caudal gantry tilt variation

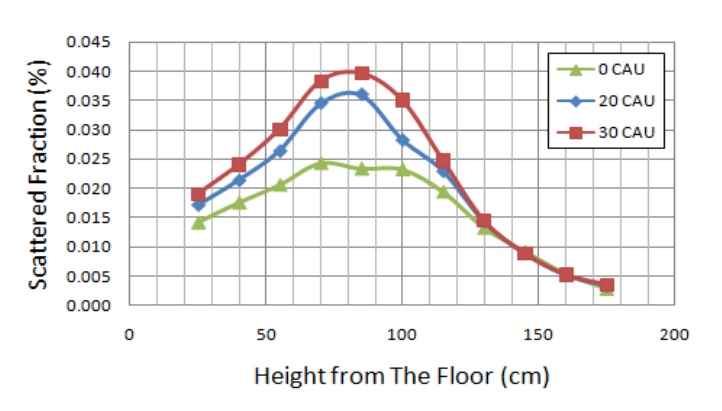


Figure 15. Graph of scattered fraction vs. the height from the floor at position 6 of caudal gantry tilt variation

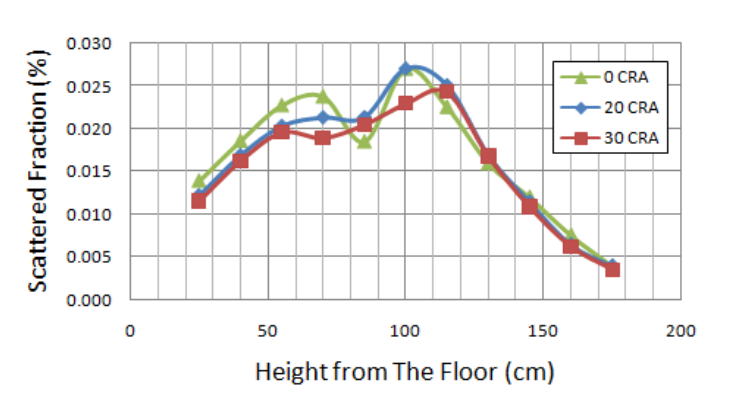


Figure 16. Graph of scattered fraction vs. the height from the floor at position 1 of cranial gantry tilt variation

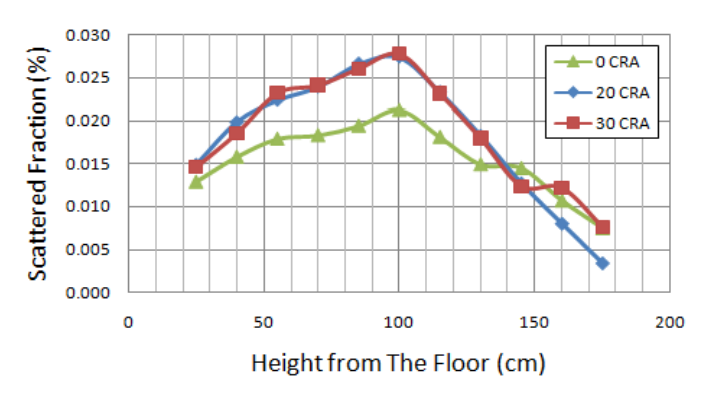


Figure 17. Graph of scattered fraction vs. the height from the floor at position 2 of cranial gantry tilt variation

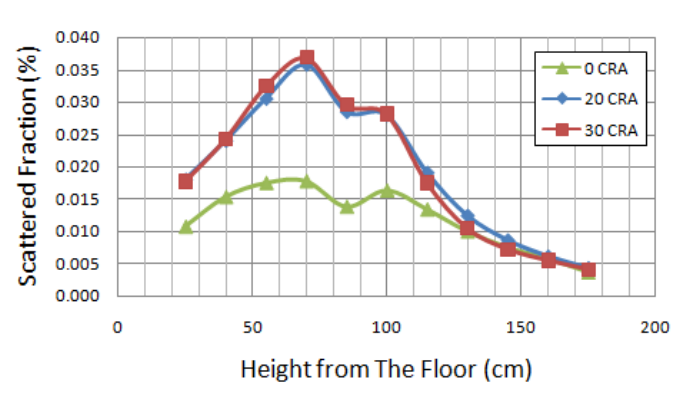


Figure 18. Graph of scattered fraction vs. the height from the floor at position 3 of cranial gantry tilt variation

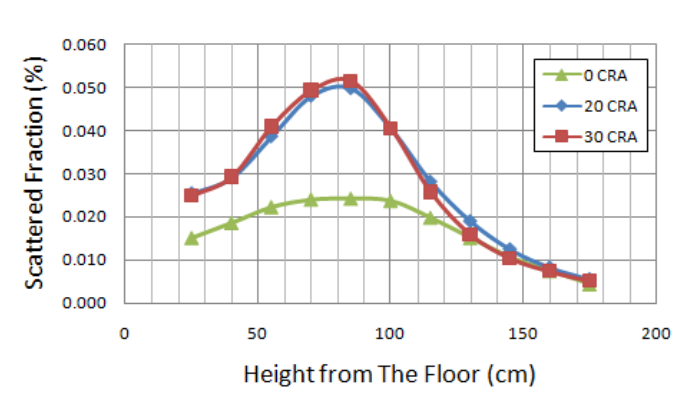


Figure 19. Graph of scattered fraction vs. the height from the floor at position 4 of cranial gantry tilt variation

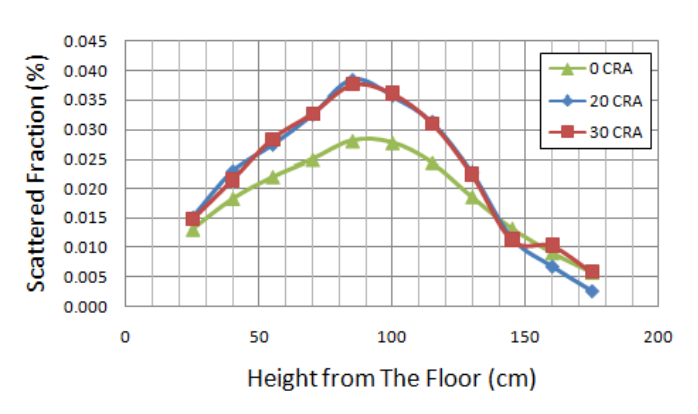


Figure 20. Graph of scattered fraction vs. the height from the floor at position 5 of cranial gantry tilt variation

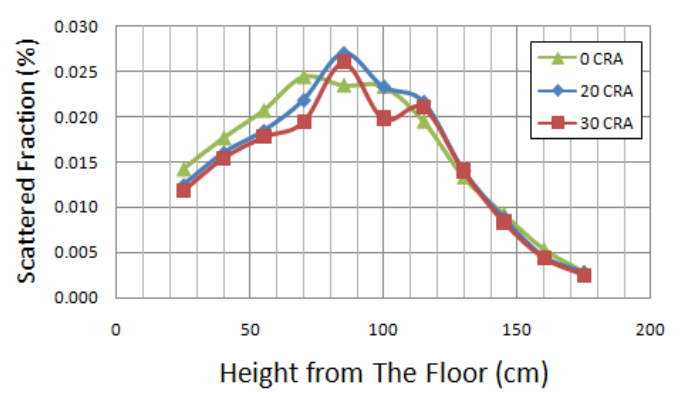


Figure 21. Graph of scattered fraction vs. the height from the floor at position 6 of cranial gantry tilt variation

IV. CONCLUSION

The scattered dose tend to increase with gantry tilt for all positions. Greater FPD size would lower the value of the scatter fraction of the dose and will minimize its scattered dose rate. The given data shown that the scattered levels are in the range of 0.001 (0.021 mGy/h) - 0.057% (1.954 mGy/h) from its primary dose at isocenter. From risk point of view, the genital organ of occupationals obtained highest scatter radiation during interventional procedures.

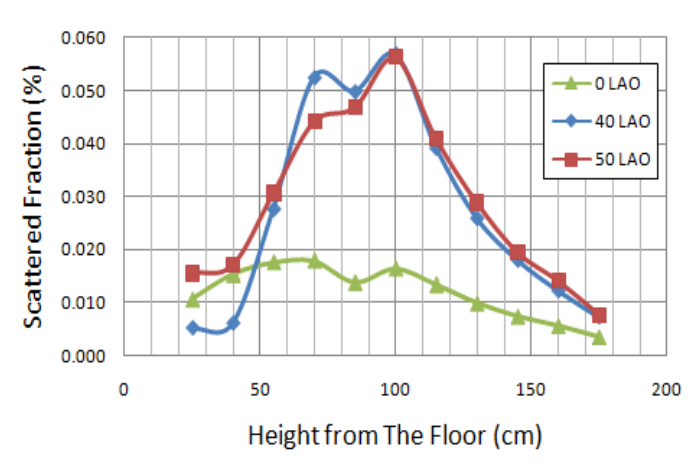


Figure 22. Graph of % relative scattering vs. the height from the floor at position 3 of LAO gantry tilt variation

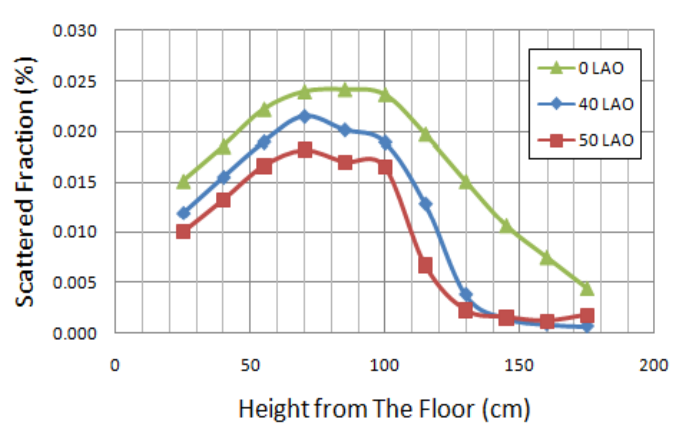


Figure 23. Graph of % relative scattering vs. the height from the floor at position 4 of LAO gantry tilt variation

REFERENCES

- Cousins, C., & Sharp, C. (2004). Medical Interventional Procedures-Reducing The Radiation Risks. Clinical Radiology, 468-473.
- [2] AAPM report No. 70, Cardiac catheterization equipment performance, Medical Physics Publishing, 2001.
- [3] Bushberg, J. T., Seibert, J. A., Leidholdt, E. M., & Boone, J. M. (2002). *The Essential Physics of Medical Imaging*. Philadelphia: Lippincott Williams & Wilkins.
- [4] Davros, W. J. (2007). Fluoroscopy: basic science optimal use, and patient/operator protection. *Techniques in Regional Anesthesia & Pain Management*, 44-54.
- [5] Domienik, J., Brodecki, M., & Rusicka, D. (2012). A Study of Dose Distribution in The Region of The Eye Lens and Extremities for Occupational Working in Interventional Cardiology. *Radiation Measurements*, 130-138.
- [6] Janne, B., & Lin, P.-J. P. (2007). The Influence of Angiography Table Shields and Height on Patient and Angiographer Irradiation During Interventional Radiology Procedures. *Cardiovasc Intervent Radiol*, 448-454.
- [7] Schueler, B. A. (2010). Operator Shielding: How and Why. Techniques in Vascular and Interventional Radiology, 167-171.

PERIPHERAL DOSE MEASUREMENT FOR 6 MV PHOTON BEAM

N.I. Mohsin, A. Zakaria, R. Abdullah, M.F. Wong

School of Health Sciences, Universiti Sains Malaysia, Kubang Kerian, Malaysia

E-mail: <u>iziana.mohsin@gmail.com</u>

Abstract: The objective of this study is to measure the peripheral dose (PD) at different depths and field sizes using film dosimetry. PD of 6 MV Siemens Primus linear accelerator photon beam for 10 cm square field and 2.5 cm diameter cone were measured at 1.5 cm and 10 cm depth, 100 cm source surface distance (SSD) with Kodak EDR2 film. PD for 10 cm square field and 2.5 cm cone were measured for the distance 1 cm to 5 cm from the geometric field edge. PD was calculated as a percentage of the central axis dose. The PD for both field sizes decreased with increasing distance from the beam edge. PD was also larger for 10 cm square field compared to 2.5 cm circular field for both depths. At 10 cm depth, the measured PD was 20% and 10% higher compared to that of 1.5 cm depth for 10 cm and 2.5 cm field size respectively. The PD for a given beam energy is a function of distance from the beam edge, field size and depth. At any depth measured, PD increases as the field size increases due to radiation scattered from the beam and scatter arising from within the medium. At deeper depth, more Compton electrons are produced and scattered to the peripheral region hence causes the PD to increase with depth. At any field size measured, peripheral dose increases as the depth increases. PD also increases as the field size increases.

Received 21 January 2014 Revised 03 February 2014 Accepted 14 February 2014 Published 28 February 2014

Keywords: Peripheral dose, EDR2 film

I. INTRODUCTION

Peripheral dose (PD) is the radiation dose received at points beyond the collimated radiotherapy field edge. In order to ensure that radiosensitive structures outside the treatment field do not receive doses approaching their tolerance levels, extensive knowledge of the magnitude and spatial distribution of the PD may be necessary [1].

Sources contributing to the total PD include the photon leakage from the treatment head of the machine, the scatter from the collimators and beam modifiers, and radiation scattered within the treatment volume [2].

Commercial treatment planning systems (TPS) should not be used to evaluate the risk of secondary cancer since they do not provide accurate modeling of peripheral dose. Differences up to 70% between TPS and Monte Carlo calculated PD was observed [3]. Another study shows that the TPS underestimated the PD by 28% to 40% as the distance from the treatment field increased and this underestimation was greater at shallow depths than at deeper depths. [4]

PD received by radiosensitive structures, such as eye lens, contralateral breast, thyroid gland, ovaries, testes, and fetus, located outside the boundaries of the primary radiation field is of clinical interest and may lead to secondary health issues [5]. Second primary malignancies occurring after radio-oncologic treatment have become a major concern during the past decade. With major improvement of long-term survival, longer follow-up, cancer registries and endresult programs, it was found that the cumulative incidence of second primary malignancies could be as high as 20% of patient treated with radiotherapy [6].

Kodak EDR2 film is relatively insensitive to x-ray energy selection, easy to process, and field size and depth had little effect on the calibration curve [7].

The objective of this study is to measure the peripheral dose at different depths and field sizes using Kodak EDR2 film

II. MATERIALS AND METHODS

All irradiations were performed by using 6MV photon beam of the Siemens Primus linear accelerator (linac) in the $30 \times 30 \times 20 \text{ cm}^3$ solid water phantom. The linac is equipped with multi-leaf collimator. The output of the linear accelerator was calibrated using IAEA TRS-398 protocol in water phantom [8].

A. Film Calibration

Kodak EDR2 films taken from the same batch were irradiated by 6 MV photon beam in the 30 x 30 x 20 cm³ solid water phantom at the centre of 10 x 10 cm² field size at depth of dose maximum (1.5 cm) with source to surface distance (SSD) of 100 cm. Calibration was carried out in perpendicular geometry for doses ranging from 25 cGy to 500 cGy. An unexposed film was developed for background reading. The dependence of the EDR2 film on depth and field size was checked. All films were processed and analyzed with Vidar Dosimetry Pro Advantage film scanner.

B. Measurement of Peripheral Dose

The peripheral dose (PD) was calculated as the percentage of dose at any depth and distance from the beam edge for a given field size to the dose in the central axis at 1.5 cm depth for the same field size. PD was measured using EDR2 film for distance 1 cm to 5 cm from the geometric field edge for 10 x 10 cm² field and 2.5 cm circular field at

both 1.5 cm and 10 cm depths. All measurements were corrected for film depth and field size dependence.

III. RESULTS AND DISCUSSION

At any depth measured, PD increases as the field size increases due to the increased intensity of the primary photon beam. Higher intensity of the primary beam contributes to higher scattered radiation. The increment is higher for the distance closer to the beam edge and is due to the scatter within the phantom from the treatment beam [2].

Table 1 shows the measured peripheral dose for 10cm square field and 2.5 cm circular cone at different depths.

Field size	10 cm 2	(10 cm	2.5 cm		
Distance from beam edge (cm)	1.5 cm depth	10 cm depth	1.5 cm depth	10 cm depth	
1	5.69	6.58	1.13	1.52	
2	3.67	4.63	0.25	0.74	
3	2.58	3.58	0.2	0.35	
4	1.99	2.67	0.19	0.23	
5	1.57	2.03	0.21	0.22	

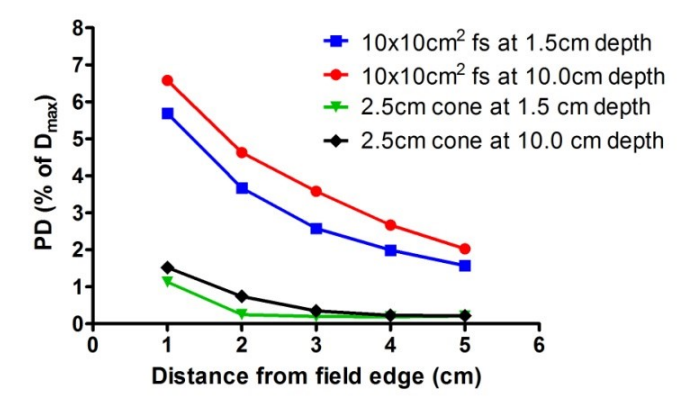


Figure 1. The measured peripheral dose for 1.5 cm and 10 cm depth for 10 cm square field and 2.5 cm circular cone.

Although the PD for both field size increases as the depth increases, the change is not as significant as the changes with field size. At deeper depth, internal (phantom) scatter dominates; causing the PD to increase with depth [9].

IV. CONCLUSION

The peripheral dose for a given beam energy is strongly dependent on distance from the beam edge, field size and depth. The measured PDs for both field sizes and for both depths decrease approximately exponentially with distance from the field edge. At any depth measured, PD increases with increasing field size. The PD also increases as the depth increases for any field size.

V. ACKNOWLEDGMENTS

The support to this research is fully funded by Universiti Sains Malaysia Fellowship Scheme.

REFERENCES

- McParland B. J., Fair H. I. (1990) A method of calculating peripheral dose distributions of photon beams below 10 MV. Med. Phys. 19:283-293
- [2] Stovall M., Blackwell C. R., Novack D. H. et al. (1995) Fetal dose from radiotherapy with photon beams: Report of AAPM Radiation Therapy Committee Task Group No. 36. Med. Phys. 22:63-82
- [3] Joosten A., Matzinger O., Jeanneret-Sozzi W. et. al. (2013) Evaluation of organ-specific peripheral doses after 2dimensional, 3-dimensional and hybrid intensity modulated radiation therapy for breast cancer based on Monte Carlo and convolution/superposition algorithms: Implications for secondary cancer risk assessment. Radiother. Oncol. 106:33-41
- [4] Howell R. M., Scarboro S. B., Kry S. F. et. al. (2010) Accuracy of out-of-field dose calculations by a commercial treatment planning system. Phys Med Biol. 55:6999-9008.
- [5] Mazonakis M., Zacharopoulou F., Varveris H. et al. (2008) Peripheral dose measurements for 6 and 18 MV photon beams on a linear accelerator with multileaf collimator. Med. Phys. 35: 4396-4402
- [6] Tubiana M. (2009) Can we reduce the incidence of second primary malignancies occurring after radiotherapy? A critical review. Radiother. Oncol. 90:4-15
- [7] Shi C., Papanikolaou N., Yan Y. et. al.(2006) Analysis of the sources of uncertainty for EDR2 film-based IMRT quality assurance. J. Appl. Clin. Med. Phys. 7:2
- [8] Technical Report Series No. 398 (2000) Absorbed dose determination in external beam radiotherapy – An international code of practice for dosimetry based on standards of absorbed dose to water.
- [9] Kase K. R., Svensson G. K., Wolbarst A. B. et. al. (1983) Measurements of dose from secondary radiation outside a treatment field. Int. J. Radiat. Oncol. Biol. Phys. 9:1177-83.

VOLUME AVERAGING CORRECTION FACTOR OF SEVERAL DETECTORS IN SMALL FIELD RADIOTHERAPY DOSIMETRY

F. Haristyo, S. A. Pawiro

Department of Physics, Faculty of Mathematics and Natural Sciences, University of Indonesia, Kampus UI Depok, 16424, West Java, Indonesia

E-mail: fajar.haristyo@yahoo.com

Abstract: Various type of detector, such as ionization chamber, has been used in small field radiotherapy dosimetry. There is a limitation in detector's dimension which can produce the volume averaging effect. Detector will average the measured dose because of fluence perturbation that happens in gas-filled cavity around detector's active volume. Purpose of this study is to calculate volume averaging correction factor of some detectors. Volume averaging correction factor can be calculated using MATLAB based algorithm. The result shows that detector with the lowest volume averaging correction factor is SFD diode detector with volume averaging correction factor value is 1,0086 in 4 cm x 4 cm field size. Whereas GD-302 has the largest volume averaging correction, 1,6083 in 0,8 cm x 0,8 cm field size. The larger size of detector, the greater volume averaging correction factor will be produced. Therefore, detector with small enough dimension is required in order to minimize the effect of volume averaging.

Received 8 February 2014 Accepted 17 February 2014 Published 28 February 2014

Keywords: volume averaging, small field, dosimetry, detector, radiotherapy

I. INTRODUCTION

Small field radiotherapy techniques, such as stereotactic or intensity-modulated radiation therapy, has been widely used in modern cancer treatment [1]. This radiotherapy technique uses small radiation field below 4 cm². Small radiation field will produce beam that conforms to the tumour target, so the healthy tissue around target can be spared.

Beside the advantages of using small field technique, there are some complications in small field radiotherapy dosimetry, for example source partial blocking that produces overlaping penumbra and the avaliability of detectors for dosimetry [2]. The output factor from LINAC will drop as the radiation field is getting smaller. The detector with large dimension will perturb the fluence on position of measurement [3]. The perturbation effect of detector is caused by the presence of gas-filled cavity inside detector resulting volume averaging effect [2].

GafChromic film is used in this study for calculating volume averaging correction factor and small beam characterization because GafChromic film is the best dosimeter for 2D dosimetry with high spatial resolution.

II. MATERIALS AND METHODS

A. GafChromic Film Calibration

Calibration data was obtained by radiating film with nine fields, 4 cm² field size with 1 cm gap between each field. The given dose for each field was varied from 0 cGy to 794 cGy [5].

Pixel value from each field was measured and converted to the determined gray value. The mean pixel value of each field was measured on MATLAB and plotted with the dose value (cGy). Afterwards, the calibration value was

interpolated with the film pixel value for both PDD and beam profile calculation.

B. PDD and Beam Profile Calculation

To obtain the PDD curve for each radiation fields on MATLAB, pixel value of film has to be measured first and then interpolated with calibration value in the form of dose value (cGy). The maximum value of interpolated dose value was normalised to 100 % representing the value of relative dose. All interpolated values were plotted against the length of the film representing depth (cm) with X axis representing depth (cm) and Y axis representing dose (%).

Similar process had been done in calculating beam profile on MATLAB. The additional process was the measurement of full width half maximum (FWHM) or actual field size. FWHM was obtained by measuring the gap between two points of 50 % relative dose on beam profile.

C. Volume Averaging Correction Factor (VACF) Calculation

VACF was determined by processing beam profile data on MATLAB. The pixel value of beam profile data was measured and interpolated with the calibration data. After being interpolated, the contour of all film pixel value representing the relative dose distribution was obtained.

The relative dose distribution was used to calculate the value of volume averaging for each detectors. The value of volume averaging was calculated by inserting the 2D dimension of detector as a border on beam profile isocenter area. All the pixel values inside the dimension border were averaged to obtain the volume averaging value. Thus, the volume averaging correction factor can be calculated using equation:

VACF = 1 / volume averaging value (1)

III. RESULTS AND DISCUSSION

A. Film Pixel Value Calibration

Film pixel value calibration had been done on two softwares; MATLAB and ImageJ. The pixel value of exposed film was determined and converted into dose value (cGy). Figures 1 and 2 show the calibration curve that was obtained by using ImageJ and MATLAB-based algorithm.

The calibration curve shows that the dose value will become smaller as the pixel value is getting greater. Polynomial equation for calibration data of 6 MV x-ray was obtained as

$$y = -0.00008x^3 + 0.0139x^2 - 79.573x + 29587$$
 (2)

while the relation of pixel value (Y) and dose value (X) on 10 MV x-ray can be expressed as

$$y = -0.0001x^3 + 0.186x^2 - 92.339x + 30240$$
 (3)

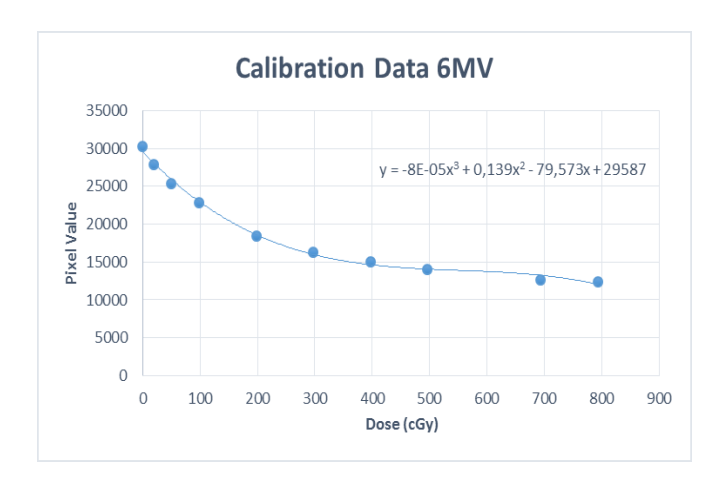


Figure 1. Pixel value calibration curve 6 MV x-ray (MATLAB)

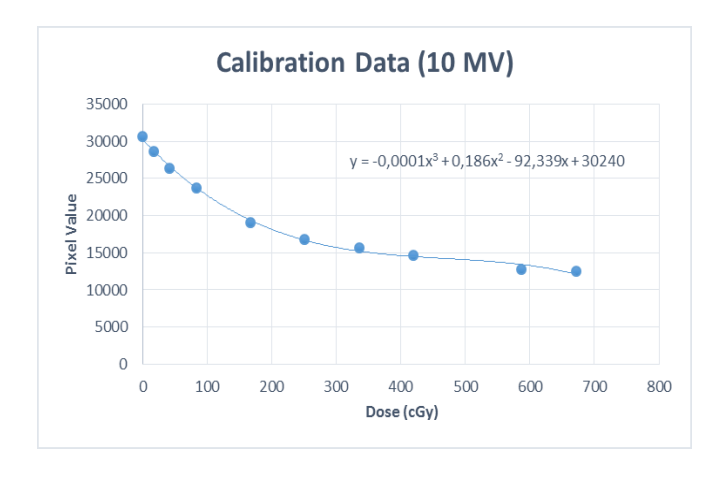


Figure 2. Pixel value calibration curve 10 MV x-ray (ImageJ)

B. Percentage Depth Dose (PDD) Calculation

PDD was calculated using MATLAB-based algorithm and compared with PDD calculation using ImageJ for validation. The resulting PDD was also compared with the result of PDD calculation using pin-point microchamber detector (Nuruddin, 2012).

1. 6 MV x-ray Beam PDD Calculation

The depth of maximum dose (d_{max}) , relative dose at depth 10 cm and 20 cm $(D_{10}$ and $D_{20})$, dose ratio at D_{10} and D_{20} , and tissue phantom ratio $(TPR_{20,10})$ of the calculated PDD was analyzed. $TPR_{20,10}$ is the absorbed dose ratio at depth 20 cm and 10 cm in water phantom measured with 100 cm SSD and 10 cm x 10 cm field size parallel with the detector [7]. TPR also represents the curve derivation exponentially after depth of maximum dose. The equation of $TPR_{20,10}$ on 10 cm x 10 cm field size is:

$$TPR_{20,10} = 1,2661 \times D_{20,10} - 0,0595$$
 (4)

The value of $TPR_{20,10}$ for small field had been determined by *Sauer et. al.*:

$$TPR_{20,10} = \frac{TPR_{20,10}^{(s)} - b_1 - A_1(1 - e^{-s/t})}{b_2 - A_2(1 - e^{-s/t})}$$
(5)

with the value of b_1 is -0,208, b_2 is 1,213, A_1 is 0,625, A_2 is -0,679 and t is 19,5.

The value of d_{max} tends to move toward surface when the field size is getting smaller [6]. But on Table 1 shows the tendency of d_{max} depending on the field size does not move consistently toward the surface. The inconsistency of d_{max} is caused by the presence of high data ripple that affects the normalising process of relative dose value. The use of high resolution (300 dpi) when scanning the GafChromic film causes quite much ripples.

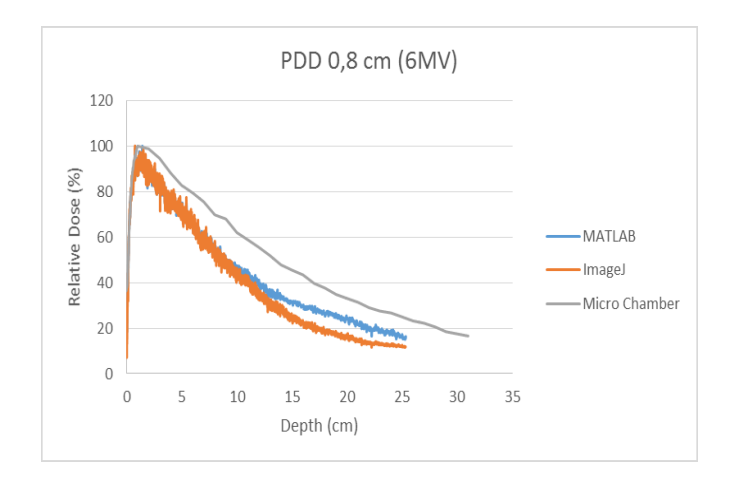


Figure 3. PDD curve (field size 0,8 cm², 6 MV x-ray).

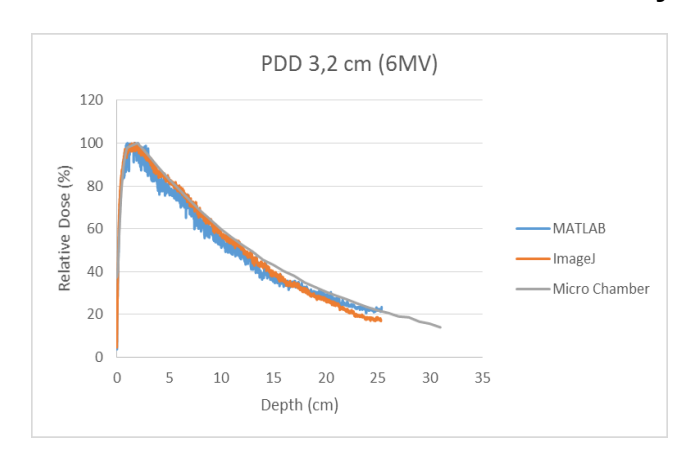


Figure 4. PDD curve (field size 3,2 cm², 6 MV x-ray).

Table 1. d_{max} and TPR_{20,10} PDD GafChromic film analysis (MATLAB)

Field Size (cm)	d _{max} (cm)	D ₁₀ (%)	D ₂₀ (%)	D _{20,10} (%)	TPR _{20,10} (Sauer) (%)	TPR _{20,10} (%)
0,8	0,74	46,39	15,8	0,34	0,62	0,46
1,6	1,23	55,58	24,33	0,44	0,63	0,56
2,4	1,42	54,86	23,93	0,44	0,63	0,56
3,2	1,69	56,94	26,66	0,47	0,64	0,59
4	1,5	58,14	23,7	0,41	0,64	0,53

Table 2. d_{max} and TPR_{20,10} PDD GafChromic film analysis (ImageJ)

Field Size (cm)	d _{max} (cm)	D ₁₀ (%)	D ₂₀ (%)	D _{20,10} (%)	TPR _{20,10} (Sauer) (%)	TPR _{20,10} (%)
0,8	1,41	46,49	24,06	0,52	0,62	0,64
1,6	1,01	55,68	26,58	0,48	0,63	0,60
2,4	1,47	51,76	26,1	0,50	0,63	0,62
3,2	1,66	56,2	28,57	0,51	0,64	0,63
4	1,31	56,07	30,06	0,54	0,64	0,65

Table 3. d_{max} and TPR_{20,10} PDD micro chamber analysis

Field Size (cm)	d _{max} (cm)	D ₁₀ (%)	D ₂₀ (%)	D _{20,10} (%)	TPR _{20,10} (Sauer) (%)	TPR _{20,10} (%)
0,8	0,99	62	33,1	0,53	0,62	0,65
1,6	1,98	58,7	29,8	0,51	0,63	0,63
2,4	0,99	60,3	30,8	0,51	0,63	0,63
3,2	1,98	59,8	30,7	0,51	0,64	0,63
4	1,98	61,8	32,1	0,52	0,64	0,64

Table 2 also shows the inconsistency of d_{max} movement tendency depending on field size. But d_{max} tends to move toward surface as field size is getting smaller (calculation with MATLAB, ImageJ and micro chamber).

The result of TPR_{20,10} calculation, shown in Tables 1 and 3, is quite similar with value range between 0,60 to 0,64. It shown that the accuracy of calculation on MATLAB is acceptable. But the calculation with ImageJ is not quite similar to MATLAB and micro chamber bercause of the interpolation order on ImageJ is smaller than MATLAB.

The mean relative error on TPR_{20,10} calculation (refering to *Sauer et. al.*) for MATLAB is 2,28 %, ImageJ is 14,58 % and micro chamber is 0,64 %.

2. 10 MV x-ray Beam PDD Calculation

Tables 4 and 5 shows the tendency of d_{max} movement toward surface as the field size becomes smaller. But there is a incongruity d_{max} value at field size 1,6 cm². It is caused by the presence of ripple on the curve that affects the measurement.

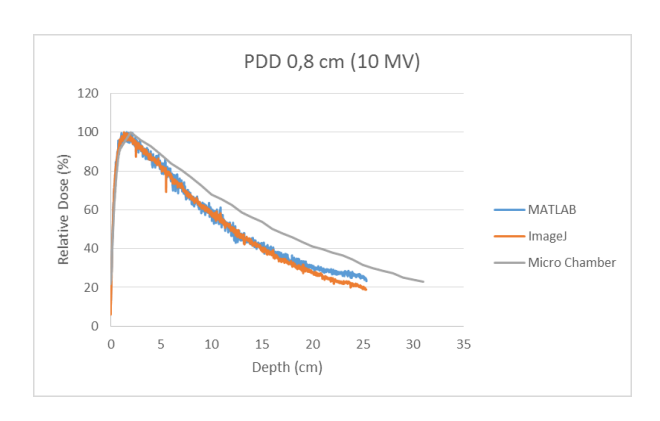


Figure 5. PDD curve (field size 0,8 cm², 10 MV x-ray)

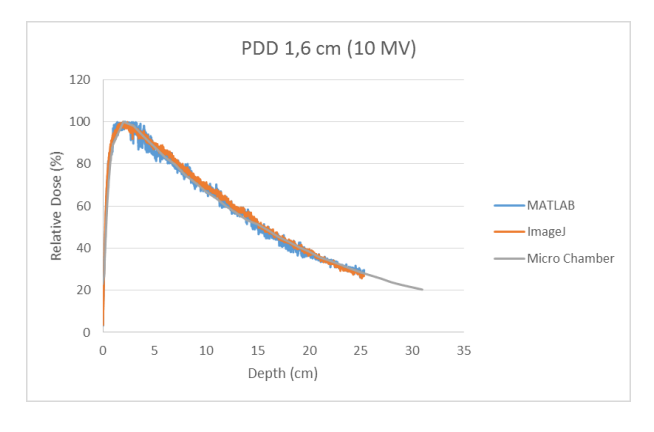


Figure 6. PDD curve (field size 1,6 cm², 10 MV x-ray)

Table 6 shown the consistency of d_{max} value in each field size. But that is not matched with Tables 4 and 5 which d_{max} tends to move toward the surface when the field size is getting smaller.

The result of $TPR_{20,10}$ on Tables 4, 5, and 6 shown consistency value range between 0,63 to 0,74. Therefore, the results of calculation using all three methods are quite similar.

The mean relative error on $TPR_{20,10}$ calculation (referring to *Sauer et. al.*) for MATLAB is 5,18 %, ImageJ is 4,31 % and micro chamber is 1,45 %.

C. Beam Profile Calculation

The calculation of beam profiles with various radiation fields has been done in this work. Beam profiles were obtained with MATLAB-based algorithm.

1. 6 MV x-ray Beam Profile

The result of 6 MV x-ray beam profile for each radiation fields is displayed on Table 4. Full Width Half Maximum (FWHM) represents the exact radiation field size. The mean deviation of the measured FWHM to the field size is 7,04 %. Whereas the mean deviation value from previous researcher (Nurrudin, 2012) is 2,3 %.

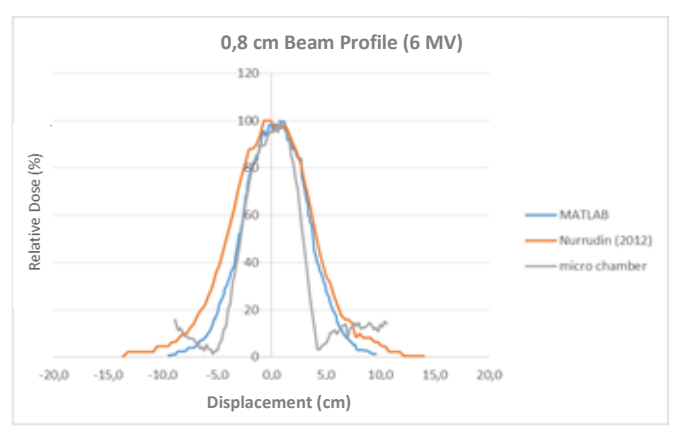


Figure 7. Beam Profile (0,8 cm²; 6 MV)

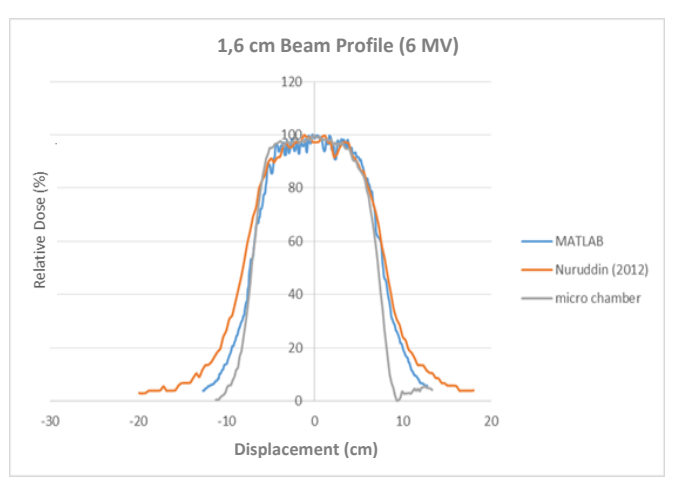


Figure 8. Beam Profile (1,6 cm²; 6 MV)

The result of penumbra measurement shown that the size of penumbra will get longer when the field size gets larger. The longer penumbra means there are numerous scattered radiation produced by large radiation field.

2. 10 MV x-ray Beam Profile

The result shown that the mean deviation of FWHM is 4,58 % while the previous research was 1,36 %. The difference is caused by the use of two different methods which are MATLAB and ImageJ. The penumbra measurement also shown the tendency of penumbra gets longer when field size is getting larger.

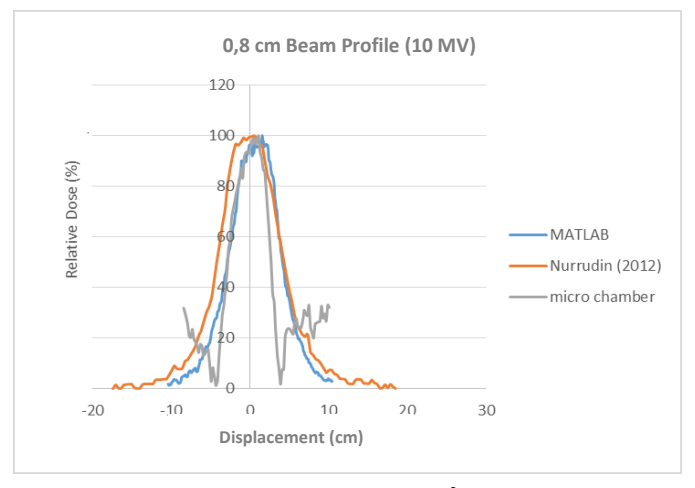


Figure 9. Beam Profile (0,8 cm²; 10 MV)

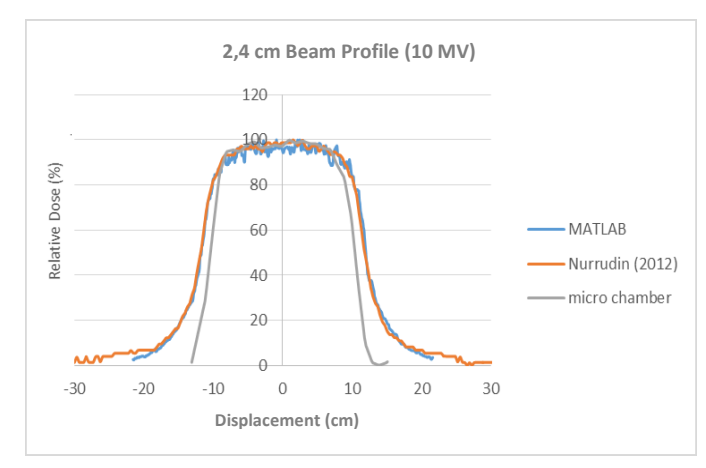


Figure 10. Beam Profile (2,4 cm²; 10 MV)

Table 4. 6 MV Beam Profile FWHM (field size) and Penumbra

	Result (MATL	AB)	Nurrudin	(2012) (ImageJ)	Nurrudin (2012) (ppmc)			
Field Size (cm ²)	m ²) FWHM (cm) Penumbra (m		Field Size (cm²)		FWHM (cm)	Penumbra (mm)	FWHM (cm)	Penumbra (mm)
0,8	0,68	3,18	0,83	3,9	0,70	2,4		
1,6	1,49	3,77	1,64	4,4	1,53	2,5		
2,4	2,29	3,89	2,36	3,0	2,36	4,8		
3,2	3,04	4,06	3,26	4,0	3,13	2,6		
4	3,85	5,17	3,92	3,1	4,00	3,2		

Table 5. 10 MV Beam Profile FWHM (field size) and Penumbra

Result (MATLAB)			Nurrudin (2	2012) (ImageJ)	Nurrudin (2012) (ppmc)		
Field size (cm ²)	FWHM	(cm)	Penumbra (mm)	FWHM (cm)	Penumbra (mm)	FWHM (cm)	Penumbra (mm)
0,8	0,71		3,51	0,77	3,8	0,74	2,6
1,6	1,54		3,64	1,61	3,8	1,53	2,2
2,4	2,33		5,33	2,37	2,8	2,32	2,6
3,2	3,12		5,33	3,23	4,6	3,11	2,5
4	3,90		5,33	3,99	5,9	3,90	3,3

D. Volume Averaging Correction Factor Calculation

Figure 11 and Figure 12 shown that the larger radiation field size, the volume averaging correction factor is nearly one. In large field size there was no overlapping penumbra read on dosimeter. The volume averaging correction factor will rise if the radiation field size got smaller. The fluence reading will be averaged by the dosimeter if the dimension of field size is very small. Therefore, the size of dosimeter must be smaller than the radiation field size in order to decrease the volume averaging effect.

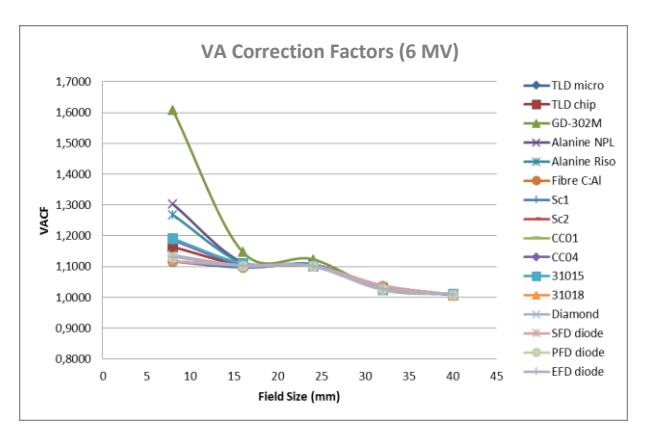


Figure 11. 6 MV Volume Averaging Correction Factor

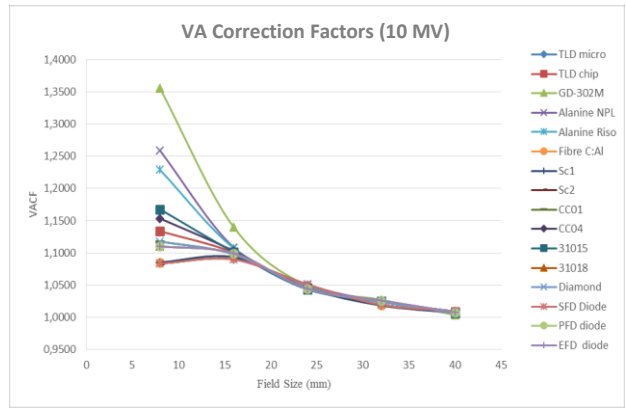


Figure 12. 10 MV Volume Averaging Correction Factor

Dosimeter with the highest volume averaging factor in the smallest field size was GD- 302M. The dosimeter has 1,5 mm x 12 mm dimension.

The volume averaging correction factor of this dosimeter is up to 1,6083. The SFD diode dosimeter has the smallest volume averaging correction factor which is up to 1,0833. The dimension of SFD diode is 0,95 mm x 0,95 mm. Therefore, the SFD diode is the most effective dosimeter for small field dosimeter.

IV. CONCLUSION

The basic algorithm for PDD, beam profile and volume averaging correction factor has been successfully developed based on the comparison of the previous research. The volume averaging correction factor will rise if the radiation field size is getting smaller. SFD diode dosimeter has the smallest volume averaging correction factor which is up to 1,0833, whereas the largest volume averaging correction factor, up to 1,6083, is on GD-302 M dosimeter.

REFERENCES

- Followill. S. D. The Radiological Physics Center's standard dataset for small field size output factors. Journal of Applied Clinical Medical Physics, Vol. 13, No. 5, 2012.
- [2] Das et. al.. Small Field: Nonequilibrium Radiation Dosimetry. Med. Phys. 35 (1), 206 215. 2007.
- [3] Aspradakis. M. M. Challenges in small field MV photon dosimetry. Cantonal Hospital of Lucerne. Lucerne. 2010.
- [4] Low et. al.. Dosimetry tools and techniques for IMRT. Med. Phys. 38, 1313-1332. 2011.
- [5] Nuruddin. Perbandingan Pengukuran PDD dan Beam Profile antara Detektor Pin Point Microchamber dan GafChromic Film pada Lapangan Kecil. Fakultas Matematika dan Ilmu Pengetahuan Alam, Universitas Indonesia. Depok. 2012.
- [6] Palta. J.R. Dosimetric Characteristics of Clinical Photon Beams. University of Florida. 2011.
- [7] International Atomic Energy Agency. Absorbed Dose in External Radiotherapy. Technical Report Series 398. Vienna: IAEA, 2000.
- [8] Institute of Physics and Engineering in Medicine. Small Field MV Photon Dosimetry. IPEM Report 103. UK. 2010.

ENTRANCE SKIN DOSE MEASUREMENT USING GAFCHROMIC DOSIMETRY FILM FOR ADULT PATIENTS UNDERGOING CORONARY ANGIOGRAPHY (CA) AND PERCUTANEOUS TRANSLUMINAL CORONARY ANGIOPLASTY (PTCA)

E. Nurtriningsih¹, K. T. Wigati¹, E. Ingrina¹, Yurneli², S. A. Pawiro¹

E-mail: endangnurtriningsih14@gmail.com

Abstract: The complexity of interventional procedures has led to increasingly longer procedure time that require significant fluoroscopic use. Fluoroscopy time is proportional to the patient dose. Once a threshold dose has been exceeded, the severity of the radiation effect at any point on the skin increases with increasing dose. The threshold dose for transient skin injuries is typically 2 Gy for erythema, the earliest detectable effect of radiation on the skin. Therefore, it is important to monitor radiation entrance exposure to the patients. Since it is not uncommon that a patient not only perform a single examination, the skin dose per examination is recommended to note if in the future radiation effect on the patient's skin arises. The skin dose records will help further treatment. The aim of this study is to evaluate patient dose in interventional radiology. Twenty one cardiac intervention procedures were studied: 12 coronary angiography (CA) dan 9 percutaneous transluminal coronary angioplasty (PTCA). The entrance surface dose were measure using DAP (dose-area product) and GafChromic XR-RV3 radiochromic film attached to the skin. GafChromic film measurement obtained the skin dose distribution on the back of the coronary area. In addition, we also measure the patient backscattering dose on the thyroid, gonad and eyes. Image analysis was performed using red channel component of standard RGB (red, green and blue) color space image. The correlation between maximum radiation surface dose and dose area product for two interventional procedures was investigated. We found a good correlation of DAP (dose-area product) and maximum entrance skin dose ($R^2 = 0.79$, $R^2 = 0.52$ for CA and $R^2 = 0.74$ for PTCA). However, fluoroscopy time seems to have a poor relationship with the patient entrance surface dose ($R^2 = 0.43$). The total irradiation time, DAP and entrance surface dose for PTCA procedures is higher than CA procedures because of the PTCA procedure is more complex. The entrance surface dose delivered to the patient can be easily measured when GafChromic films are used. The GafChromic dosimetry allows precise mapping of the skin dose distribution, when placed close to the skin. The GafChromic film results that the radiation dose to the surface for PTCA procedure greater than CA.

Received 8 February 2014 Accepted 21 February 2014 Published 28 February 2014

Keywords: interventional radiology, entrance skin dose, angiography, angioplasty, GafChromic

I. INTRODUCTION

Nowadays, interventional radiology techniques and the equipment are more advanced, but the possibility of patients exposed to high radiation doses cannot be avoided. This, of course, can lead to deterministic and stochastic effects of radiation exposure. Symptoms of radiation effects are commonly found in patients with long fluoroscopy time. The effect of radiation on the body that occurs after a dose threshold is exceeded on the portion of the patient's skin, the severity on injury at that point increases with increasing dose, called deterministic effects [1].

Short-term effects that may occur from interventional cardiology procedures is the appearance of erythema (redness symptoms of skin tissue) and necrosis (tissue death) of the skin [5]. Radiation effects at any point on the skin equivalent the doses of that point. Reducing the maximum skin dose can reduce the likelihood and type of skin injury, such as minimizing fluoroscopy time and number of cine, and controlling technical factors. Levels of skin damage caused by radiation depends on several factors which include the

type of radiation, the radiation dose rate, the radiation-exposed area of the skin and the skin characteristics. Since 2 Gy is used as the threshold for early detection of the radiation effect on the skin, the management of patient dose is important. However, the actual threshold dose of radiation required to cause skin damage varies among individuals, influenced by the level of individual biological radiation sensitivity and the disease that causes the skin to be more sensitive to radiation such as diabetes, genetic disease ataxia telangiectasia and connective tissue disorders [2].

Radiographic film is a method for dose monitoring during fluoroscopy and it can be used over a broad area [6]. The dosimetry film, GafChromic XR-RV3 is specially designed for measuring skin dose distribution using fluoroscopy in interventional procedures, with the size of 14" x 17" with the energy range 30 keV - 30 MeV (ISP GafChromic). From measurement, it was obtained skin dose distribution and maximum skin dose at the back area of the body, especially the coronary areas and organ at risk doses. Color change in the film can be measured with GafChromic dosimetry densitometer, scanner or spectrophotometer.

^{1.} Department of Physics, Faculty of Mathematics and Natural Sciences, University of Indonesia, Kampus UI Depok, 16424, West Java, Indonesia

² Cath Laboratory, Harapan Kita Cardiac Hospital, Jakarta, Indonesia

In interventional radiology, patient dose and estimation of effective dose can be obtained from measurements of the dose-area product (DAP) [3,4]. Based on that investigated the correlation between DAP and entrance skin dose, we also evaluated the relationship between DAP value and maximum skin dose in GafChromic.

II. MATERIALS AND METHODS

The study was carried out from April to May 2013 in the cardiac catheterization lab, National Cardiovascular Center, Harapan Kita Hospital, and included 20 patients who underwent interventional cardiology procedures. Measurement procedure was limited in adult patients Coronary Angiography (CA) and Percutaneous Transluminal Coronary Angioplasty (PTCA), respectively, 10 patients with a variety of radiation field size, the number of frames and fluoroscopy time. The doses was influenced by the fluoroscopy time, thickness of patient, the field size and the number of radiographic frames.

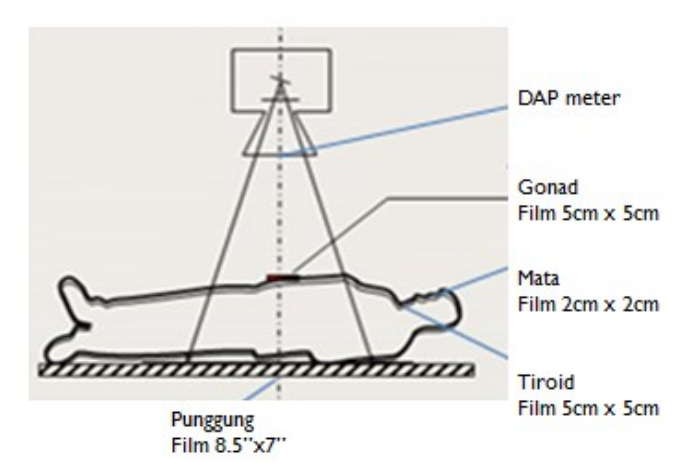


Figure 1. Measurement method

Cath lab room 1, 3 and 5 (R1, R3 and R5) were used for this study. Room 1 and 3 uses the Philips Integris Allura Xper FD10 (Philips medical systems) while Room 5 uses Innova (General Electric, Milwaukee WI, USA). While in use, fluoroscopy device's voltages and currents are regulated by a system of automatic exposure control (AEC). For each examination we recorded the fluoroscopy time, DAP value, number of sequences and cine frames per sequences, dose rate and field size. All procedures were carried out by invasive cardiologist.

Patient dosimetry measurements were performed using dose-area product (DAP) and the GafChromic XR-RV3 radiochromic film. It used Diamentor M4 system (PTW Freiburg), which includes a transmission ionization chamber attached to the collimator exit port of the x-ray tube, placed perpendicular to the beam central axis and located around the area to intercept the x-ray beam. Radiation dose is measured from the contribution fluoroscopy and cine radiography. Different from dap, GafChromic method only provides dose data post procedurally and therefore, this method may be more advantageous when used with other monitoring

methods to better determine the actual area of exposure because it placed attached to the skin [6].

Because of the sensitivity of the organs to radiation varies, organs and tissues of the body has a different radiation dose threshold. Group of organs that are very sensitive to radiation than the skin such as gonad, thyroid, and eye. Therefore, in this study we also measured skin entrance dose to the gonads, eye and thyroid patients, also using GafChromic. Entrance skin dose measurement used GafChromic film in dimension 17" x7". As for the risk of organ dose measurements used for thyroid and gonads are 5x5 cm and for eye 2x2 cm.

Twenty consecutive patients cardiac intervention procedures were studied: coronary angiography and percutaneous transluminal coronary angiography. For entrance skin dose measurement, 5 coronary angiography (3 men, 2 women) and 6 PTCA patients (11 men, 4 women) were used. For organ at risk: eyes, gonad and tiroin measurements, we were used all patients (14 men, 6 women).

III. RESULTS AND DISCUSSION

A. DAP Conformance Test

To ensure that DAP in fluoroscopy work accurately, necessary to test the suitability of DAP in advance. DAP conformance testing is done by finding the DAP calibration factors used by the DAP has been calibrated. Therefore, the measurement used three different fluoroscopy in three different rooms, performed DAP conformance testing on each room

Table 1 shows the value of the DAP calibration factor is obtained. Each calibration factor of the rooms is different, 1.12; 1.24; 1.64 for R1, R3 and R5, respectively. The maximum DAP calibration factors is in R5 (room no. 5), indicating that the lowest accuracy of DAP at room no. 5. Of all the DAP calibration factors, it is known that the DAP in the three rooms need to be recalibrated, especially room no. 5, which presented the highest calibration factor of 1.64.

Table 1. DAP calibration factors of each room

DAP R1	1.1156
DAP R3	1.240
DAP R5	1.64

B. Patient Data Analysis

Of the total 11 patients who underwent entrance surface dose measurements, 5 CA and 6 PTCA, the data measurement obtained in Table 2. The data consists of irradiation factor, total fluoroscopy time and total DAP for each examination.

Total fluoroscopy time was the total of fluoroscopy and cine time. The total fluoroscopy time varied for each patient and was affected by several factors such as the complexity of the procedure, the type of procedure, the structural characteristics of the patient's anatomy, and work experience the interventionist.

				Exposure Factors		etors		
No. of patient	Procedure	Sex	Weight [kg]	kV	mA	ms	Total fluoroscopy time [min]	Total DAP [cGy.cm ²]
1	CA	P	38	67	351	4	12.78	2806
2	CA	L	65	85	878	7	12.25	9614
3	CA	L	70	96	6	5	10.38	7662
4	CA	L	73	80	897	8	6.95	3544
5	CA	L	72	80	18.7	6	5.62	2671
6	PTCA	P	58	72	704	6	20.83	15184
7	PTCA	L	65	100	11.9	7	8.55	5320
8	PTCA	L	62	86	18.5	7	28.22	25926
9	PTCA	L	61	100	12.8	6	29.48	19303
10	PTCA	L	52	80	17.2	7	6.47	5556
11	PTCA	P	51	78	18.2	7	46.38	16219

Table 2. Measurement data of CA and PTCA procedures

Complexity of the procedure allows the use of multiple projections needed to do varying illumination geometry. This can be seen in Figure 2, the post-irradiation GafChromic films in the measurement of patient no. 8, beam irradiation on the film looks not only at one area but some areas, in fact, there is absence of field overlapping. The use of projection geometry is to avoid the buildup of radiation dose at only one point / area that can lead to the possibility of erythema when cumulative doses exceed the dose limit of 2 Gy. In a single procedure conducted, the FDA (Food and Drug Administration) suggest that the cumulative dose at a point not more than 1 Gy.

Of each procedure, total DAP values constitutes the combined fluoroscopy dose and cine contribution. For imaging optimization, each patient's radiation factor tube voltage and current are varied. This is because in the cardiac catheterization, the use of kV and mA is set automatically by the ABC (Automatic Brightness Control) based on the thickness of the patient's body. The differences of the body thickness produces backscattering radiation which is also different. The thicker the body, backscattered dose will be greater. The greater backscattered radiation certainly raise the entrance surface dose.

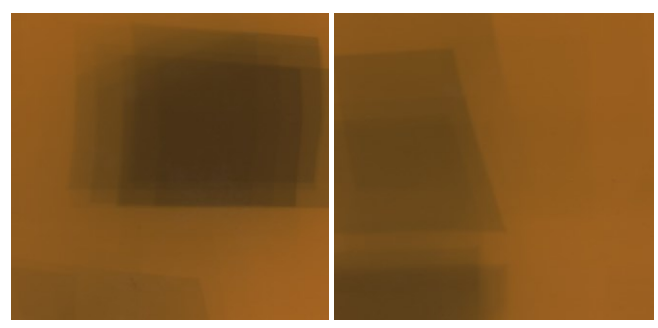


Figure 2. Post-irradiation films of patients no. 8 and 11

From Table 3, note the value of the maximum ESD for each examination. The maximum ESD values characterized in bold, for CA procedures was 29.54 cGy whereas PTCA

was 208.06 cGy. Entrance dose of 208.06 Gy is clearly dangerous for patients because it has exceeded the threshold of the radiation effects erythema (redness symptoms of the skin). Therefore, the hospitals are encouraged to give special attention to cardiac catheterization especially PTCA. Catheterization team expected to record the medical data of the radiation dose received by the patient so that when later the biological radiation effects occur in patients can be dealt with appropriately.

After the films were analyzed using Matlab software, the entrance surface dose distribution as shown in Figures 10 and 11. Figure 10 shows dose distributions of patient no. 8 with a total fluoroscopy time 28.22 min, DAP 321.49 Gy.cm² and the maximum entrance dose 208.06 cGy. Figure 11 shows dose distributions of patient no. 11 with a total fluoroscopy time 46.38 minutes, DAP 265.50 Gy.cm² and maximum entrance dose 92.97 cGy. From the differences in both fluoroscopy exposure duration, even though the patient no. 11 had longer fluoroscopy time than patients no. 8, but the maximum entrance doses patients no. 8 was greater. It is informed that the total fluoroscopy time was not the only one of factor that influences the patient's entrance dose.

In Table 3 is also known that the PTCA procedure average of the total fluoroscopy time is higher (23.32 min) than in CA (17.08 min). Neither the average of DAP and average of maximum ESD, for both greater in PTCA procedures (195.26 Gy.cm² and 93.02 cGy) than CA (72.73 Gy.cm² and 34.88 cGy). In the PTCA procedure, the DAP and ESD is greater than CA because of PTCA is more complex; it does not only look at the position of the heart artery blockage but also open the blockage treatment with / without stent. As a result of course fluoroscopy time in the PTCA procedures are longer than the CA, so the DAP and ESD will be greater in PTCA procedures.

From the graph of the correlation between the maximum entrance dose and total fluoroscopy time in the procedure CA (Figure 4) shows that the linearity less significant ($R^2 = 0.24$) or it can be said that the relationship is not linear. Likewise PTCA procedures (Figure 5), both linearity relationship was not significant ($R^2 = 0.27$). However, when seen from the whole procedure (Figure 6), the correlation between

Table 3. DAP and maximum ESD measurable

Patient	Procedure	Total fluoroscopy time [min]	DAP corrected	MSED [cGy]
1	CA	12.78	3130.60	19.83
2	CA	12.25	11921.36	75.9
3	CA	10.38	12543.84	33.2
4	CA	6.95	4395.68	29.54
5	CA	5.62	4372.43	15.93
6	PTCA	20.83	18828.78	62.40
7	PTCA	8.55	6597.05	52.49
8	PTCA	28.22	32148.98	208.06
9	PTCA	29.48	23935.84	118.27
10	PTCA	6.47	9095.17	24.94
11	PTCA	46.38	26550.50	91.97

maximum entrance dose and total fluoroscopy time was more significant ($R^2 = 0.43$). From this information, it can be seen that although the correlation between entrance surface dose with the fluroscopy time is less linear ($R^2 = 0.43$), the increase of fluoroscopy time tended to increase the entrance surface dose.

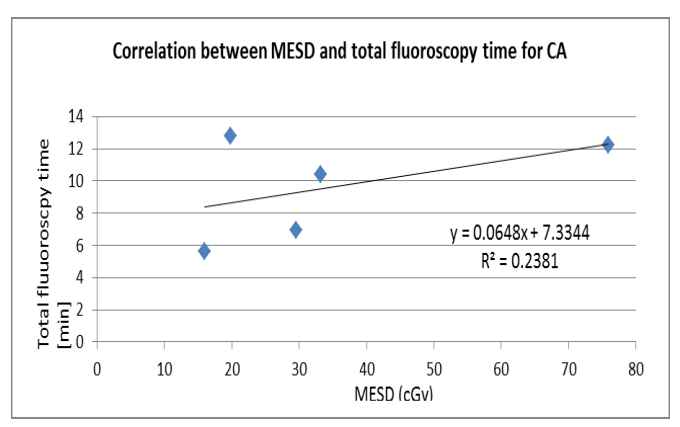


Figure 4. The correlation between MESD and total fluoroscopy time for CA

Figure 7 shows the correlation between the DAP and maximum entrance surface dose for CA procedure. Although both of them shown less linear relationship ($R^2 = 0.52$), but it appears that DAP tend to increase with increasing the entrance surface dose. While the correlation of DAP and maximum entrance surface dose for PTCA procedure (Figure 8), the relationship has more significant linearity ($R^2 = 0.74$). The graph of DAP and maximum entrance surface dose for the entire procedure (Figure 9) shows a significant relationship ($R^2 = 0.79$). This graph informs that the increase the entrance surface dose is directly proportional to increase in DAP. This is because the DAP is air Kerma dose from source multiplied with the field of radiation, while the dose entrance is the total the air Kerma dose and backscattered dose. So both of them has directly proportional relationship.

Table 4. Mean values for DAP, the maximum ESD and total fluoroscopy time

Procedure	Mean DAP [Gy.cm2]	Mean MESD [cGy]	Mean total fluoroscopy time [min]
CA	72.73	34.88	17.08
PTCA	195.26	93.02	23.32

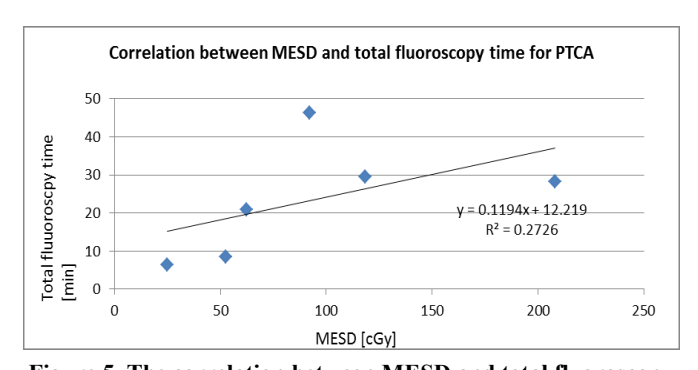


Figure 5. The correlation between MESD and total fluoroscopy time for PTCA

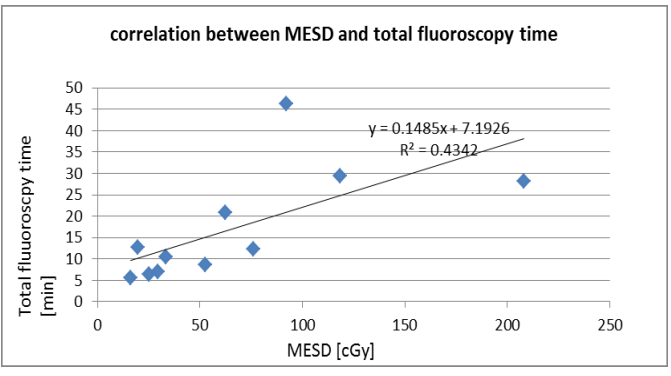


Figure 6. The correlation between MESD and total fluoroscopy

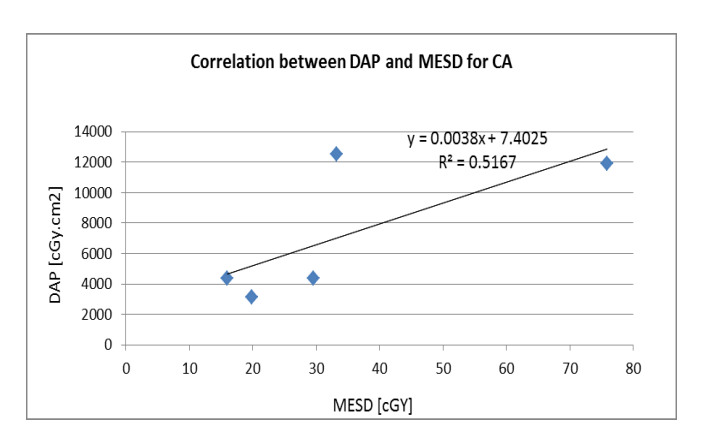


Figure 7. The correlation between DAP and MESD for CA

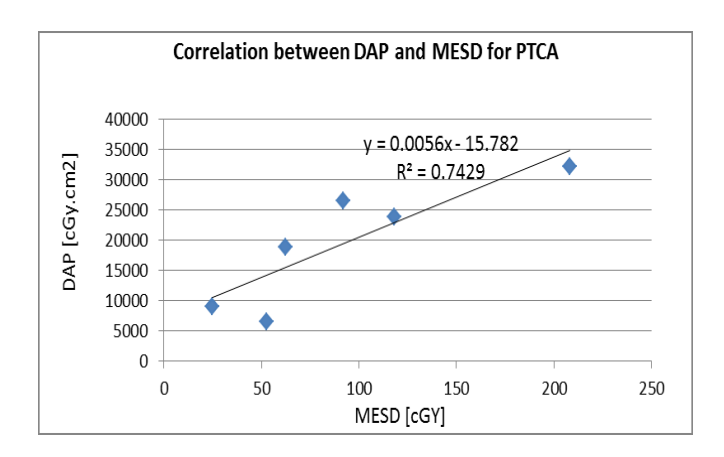


Figure 8. The correlation between DAP and MESD for PTCA

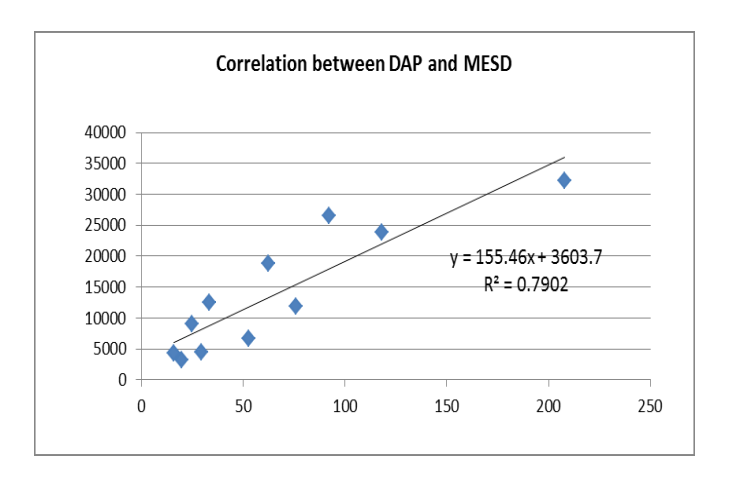


Figure 9. The correlation between DAP and MESD for PTCA

C. Organ At Risk Dose

The entrance surface dose measurements on the Organ at Risk (gonadal, thyroid and eye) was performed in 21 patients undergoing cardiac catheterization. Overall patients observed were 12 CA and 9 PTCA. ESD is recorded in Table 5. Entrans dose is the backscattering radiation dose because the point are not on the primary radiation beam. Entrance dose distribution for all patients can be seen in Figure 7, displayed entrance dose on eyes, gonads and

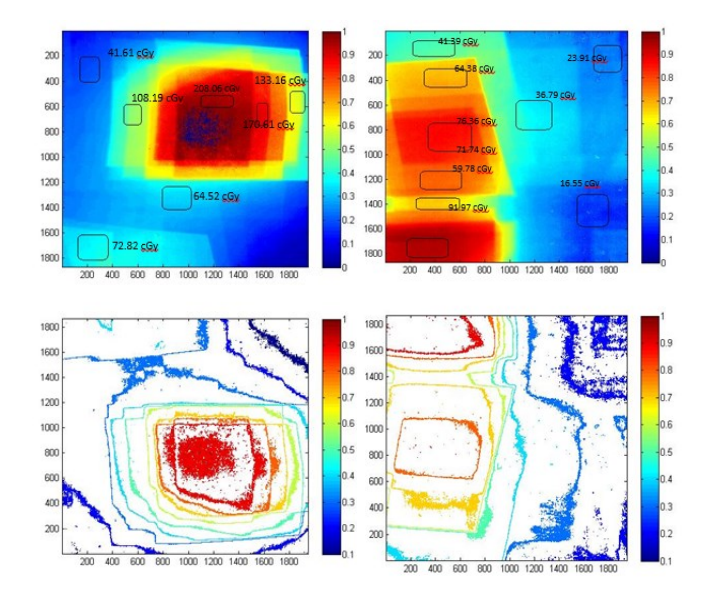


Figure 10. Radiation dose distribution of patient no. 8 (left) and patient no. 11 (right)

thyroid. Each patient received a different entrance dose of OAR. For the eye, the highest dose is 2.63 cGy in the patient no.4. As for the gonads and thyroid, the highest entrance dose received by the patient no. 10, 2.93 cGy and 3.67 cGy. Overall the thyroid received the highest of backscattering dose (2.34 cGy) compared to the gonads (1.83 cGy) and eyes (1.49 cGy). This is because the location of the thyroid that is closest to the heart so that it gets the maximum backscattering radiation.

Table 5. ESD on gonadal, thyroid and eye

D 41 4	Exposure factor			Entrance Dose [cGy]		
Patient	kV	mA	ms	Eye	Gonadal	Thyroid
1	79	867	7	2.53	2.67	3.25
2	74	17	7	0.67	1.99	2.75
3	81	899	7	0.97	1.85	2.75
4	98	19	7	2.63	2.63	3.15
5	93	19	7	1.67	2.21	1.85
6	81	70	5	0.49	0.18	2.05
7	68	394	5	0.31	1.50	2.10
8	81	19	7	2.16	1.45	3.68
9	83	19	7	0.23	1.70	2.68
10	78	19	7	1.08	2.93	3.67
11	67	351	4	1.82	1.57	1.11
12	72	704	6	1.25	2.46	1.41
13	85	878	7	0.55	2.63	3.03
14	100	12	7	2.36	2.66	1.65
15	86	19	7	1.65	1.19	2.09
16	96	6	5	2.45	2.45	2.02
17	80	897	8	0.79	2.29	2.60
18	100	13	6	2.35	2.65	2.61
19	80	19	6	1.12	0.00	2.20
20	80	17	7	2.59	1.00	1.81
21	78	18	7	1.68	0.36	0.63
	Mea	ın		1.49	1.83	2.34

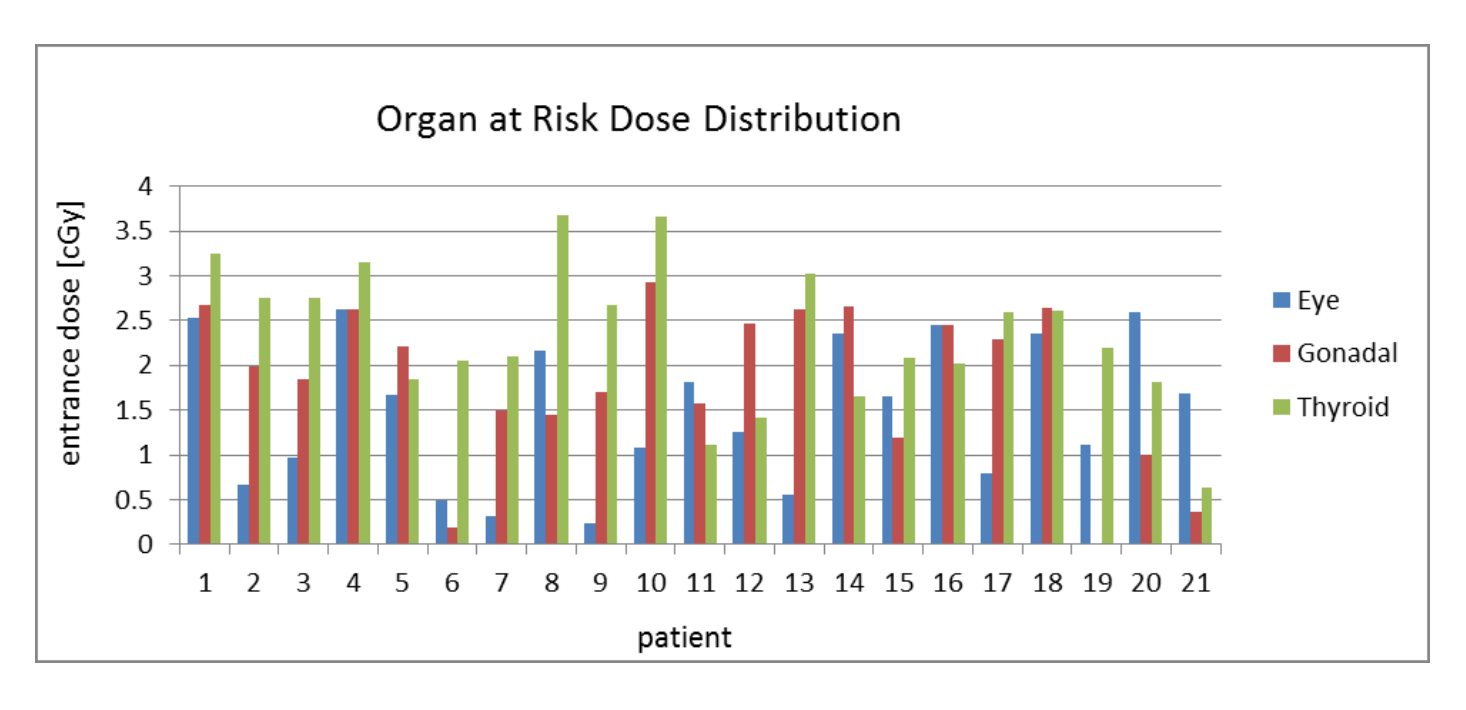


Figure 12. ESD distribution on gonadal, thyroid and eye

IV. CONCLUSION

The entrance surface dose delivered to the patient can be easily measured when GafChromic films are used. The GafChromic dosimetry allows precise mapping of the skin dose distribution when placed close to the skin. The GafChromic film results that the radiation dose to the surface for PTCA procedure greater than CA.

REFERENCES

[1] Koenig TR, Wolff D, Mettler FA, Wagner LK. Skin Injuries from fluoroscopically guided procedures. I. Characteristic of Radiaton

- [2] Wagner LK, McNeese MD, Mark MV, Siegel EL. Severe skin reactions from interventional fluoroscopy: case report and review of the literature. Radiology 1999; 213:773-776.
- [3] Stratis Andreas, Anthopoulos Prodromos, et al. Patient dose in cardiac radiology. Hellenic J Cardiol 2009: 50: 17-25.
- [4] Hart D, Jones DG, Wall BF. Estimation of effective dose in diagnostic radiology from entrance surface dose and dose-area product measurements, Report NRPB-R262. London: HMSO, 1994.
- [5] International Commission on Radiological Protection publication 85: avoidance of radiation injuries from medical interventional procedures.
- [6] Technical white paper: Monitoring and tracking of fluoroscopic dose. December 2010.

HOW TO PUBLISH IN JOURNAL OF MEDICAL PHYSICS AND BIOPHYSICS: AN AUTHOR'S WRITING GUIDELINE

<u>Authorname Authorsurname</u>¹, Coauthorname Coauthorsurname², Coauthorname Coauthorsurname^{2,3}, and Coauthorname Coauthorsurname^{1,2}

- ^{1.} Institution name, address
- ^{2.} Institution name, address
- 3. Institution name, address

E-mail: editor@jmpb.org

Abstract: The abstract should be clear, descriptive and no longer than 250 words. It should provide a brief introduction to the problem. A statement regarding the methodology should generally follow a brief summary of results. The abstract should end with a comment on the significance of the results or a brief conclusion. Abstract is written in Times New Roman font, 10 pt sized.

Received Revised Accepted Published

Keywords: Minimum 3 and maximum 5 words which are not contained in the title

I. INTRODUCTION

This author kit is designed to assist authors in preparing their submission to Journal of Medical Physics and Biophysics. It is an exact representation of the format expected by the board of editor for the final version of papers. Final submissions not following the required format will be returned to the authors for modification and compliance.

One can simply edit the document you are now viewing. Formats of paper components are available as styles along with this file. All scientific papers to be submitted should be written in English.

II. MATERIALS AND METHODS

This section provides information on how submitted papers should be arranged technically. It also serves as an exact example for writing.

A. Submission method

Colleagues who wish to publish their works should submit the full manuscripts (maximum 10 pages). Journal of Medical Physics and Biophysics is issued on February and August annually.

Authors must submit their work electronically, by electronic mail after completing online submission procedure. The acceptable formats are Microsoft Word for Windows (any version) or RTF (Rich Text Format). No PDF format is to be accepted for submitting.

B. Submission steps

- Download the file "Writing Guideline for Authors.docx" from the web site http://jmpb.org. Open the file with MS word 2007 or later version.
- Modify the file. Replace the existing text (e.g. title, authors, text, figure, table, references etc.) with your text. Papers should be maximum ten pages.

- Rename the final paper file using a new name. The final paper filename should have the following name: Author.doc where Author is the corresponding author's name and doc denotes that the document is in MS Word.
- Complete the online submission procedure found at http://jmpb.org after registering yourself as author.
- Any inquiry should be addressed by e-mail to editor@jmpb.org.

The remaining of this document describes the format requirements to which final accepted contributions should adhere.

C. General organization of the paper

It is recommended that Scientific Papers have explicit sections for Introduction, Material and Methods, Results and Discussion, Conclusion, and Acknowledgements (when applicable).

D. Document format

A number of paragraph styles have been created to facilitate the formatting of the document. If using Microsoft Word, this template will help in matching the requirements for the submissions.

The paper size is A4 (210 x 297 mm), double-column format with a 0,5" margin at all sides. Spacing between columns is 0,3". Lines are single spaced, justified. Do not number the pages and do not include references to page numbers in the text.

1. Headings

Use only a maximum of three levels of heading as follows:

- Level 1 13 pt, Arial bold, left-aligned, sentence case, roman numerical-numbered
- Level 2 12 pt, Arial italics and bold, left-aligned, sentence case, capital latin-numbered
- Level 3 10 pt, Times New Roman, bold, left-aligned, sentence case, arabic-numbered.

Authorsurname, et al.

Use bullets as in the next section. Ensure that page breaks do not come between any heading and the next level of sub-heading or first line of body text after the heading (in Word, use paragraph formatting of 'Keep with next' for Line and Page Breaks on heading lines). When MS. Word is used, authors are encouraged to follow the formatting (styles) for corresponding paragraph parts and components.

2. Body text

The font used throughout the paper is Times New Roman 10 pt. Standard paragraph has no space both before and after the paragraph. Do not include extra paragraphs between lines. Body text format applies under all headings. All spacing must be set at an increment of 12 pt.

3. Bullets

There are two levels of allowed bulleting:

- This is the first bullet level. Font is Times New Roman 10 pt, with no space before and after the paragraph. Paragraph is hanging by 0,48 cm and text starts at 0,67 cm from the margin.
 - This is a sub-bullet level. Font is Times New Roman 10 pt, with no space before after the paragraph. Paragraph is hanging by 0,4 cm and text starts at 1,19 cm from the margin.

For texts requiring additional bullets level to be created, a table showing the complete data is advisable rather than the use of multiple bullets.

4. Tables

Tables are sequentially numbered in numeric fashion with the table number and the title above the table. Caption font is Times New Roman 9 pt bold, with no space before and 12 pt space after the paragraph. Include a paragraph immediately after the table to separate it from the following text or heading.

Tables should be centred in the page. Font is Times New Roman 9 pt, with 6 pt space before and 6 pt space after the paragraph. Table column headings should still use the same style but be bold. Tables are referred to in the text by the table number as shown in Table 1. When necessary, tables can be made wide accross the two columns.

Object	Font	Align
Paper Title	14 pt Arial, bold, upper Chase	Left
Abstract	Times New Roman font, 10 pt	Justified
Text body	10 pt Times New Roman,	Justified
	sentence Chase	
Heading 1	12 pt, Arial bold, left-aligned,	Left
	sentence case, roman	
	numerical-numbered	
Heading 2	11 pt, Arial italics and bold, left-	Left
	aligned, sentence case,	
	capital latin-numbered	
Heading 3	10 pt, Times New Roman, bold, left-	Left
	aligned, sentence case	
Bullet	Times New Roman 10 pt	Justified
Sub-bullet	Times New Roman 10 pt	Justified

5. Figures

Figures are sequentially numbered in numeric fashion with the table number and the title below the figures. Caption font is Times New Roman 9 pt bold, with no space before and 12 pt space after the paragraph.

Figures should be centered in the page. The size of the figure must be kept proportional (not stretched) and span at exactly the column's width (8,72 cm). Font is Times New Roman 8 pt, with adjustable (increment of 12) space before and fixed 12 pt space after the paragraph. Figures are referred to in the text by the figure number. Figure 1 shows an included object.

Detailed recommendations for figures are as follows:

Ensure that figures are clear and legible. Black & white only is allowed. Hard copy illustrations should be scanned and included in the electronic version of the submission in an appropriate manner.

Acceptable formats as follows:

- BMP Microsoft bitmap file
- WMF Windows Metafile Format
- JPG JPEG File Interchange Format
- TIF Tagged Image File Format
- GIF
- PNG

The following included files are also permissible:

- Microsoft Graph
- Microsoft Draw
- VISIO Draw

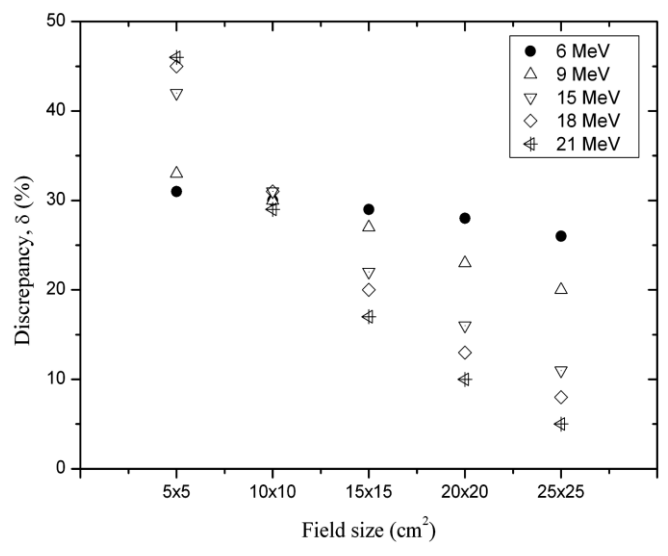


Figure 1. An example of figure

6. Equations

Equations are sequentially numbered in numeric fashion with the equation number and no title above or below the equation. Equations to be identified with bracketed decimal number right-justified after the equation. Should this is impossible (equation too long), bracketed denotation to be made in the same fashion right below the equation.

Font is Times New Roman 9pt bold, with 24pt space before and 24pt space after the paragraph. Should the equation spans longer that the spaces are cutting the

Authorsurname, et al.

equation's top or bottom side, the spacing must be modified into any increment of 12 to maintain vertical alignment between inter-column lines.

$$\delta = \left| \frac{D_{calc} - D_{meas}}{D_{meas}} \right| \times 100\% \tag{1}$$

7. References

All publications cited in the text should be included in a list of references as the last section of the paper. Within the text, references must be denoted by placing number of appearance order between square brackets [1].

Two or more different references addressing the same ideas should be indicated by putting all references between a pair of square brackets, separated by comma [2,4,6,7]. Order of appearance should be made on the references section.

List of references should serve as an enclosure for the entire paper. The format accepted for publication is a modified APA format, where they are being numbered by the order of appearance rather than sorted alphabetically without number as the original APA style is.

III. RESULTS AND DISCUSSION

Submissions for Full Paper will be reviewed by the board of reviewers. Reviewers will use a standardized form for review. Evaluation will stress the originality of the submission, the contribution to medical physics and biophysics field, the clarity of exposition and the adequacy of references to relevant work.

All accepted papers will appear on the website of the Journal of Medical Physics and Biophysics. Printed version can be requested by sending an inquiry to editor@jmpb.org mentioning the issue number or subscription request. Authors may wish to include a letter to the Editor with their final

submission if the final Full Paper makes a major deviation from these expectations.

IV. CONCLUSION

A detailed conclusive remarks should be included in this section. Further recommendation and statements may also be involved.

V. ACKNOWLEDGMENTS

When necessary, this section serves as a media to thank those that have supported you and your work.

REFERENCES

- [1] International Reference Writing Agency. (2004). *How to Write Reference List Properly*. Cityname: References Press.
- [2] JMPB Editor. (2013). How to Publish in Journal of Medical Physics and Biophysics: An Author's General Guideline. *J. Med. Phys. Biop.*, *I*(1), 1-3.
- [3] Lastname, F. M. (2000). Book Title. City: Publisher.
- [4] Lastname, F. M. (2011). Putting References with the Right Manner. In F. M. January, & Q. J. King, *Writing an Article May Not Be Difficult* (pp. 234-270). Cityname: Publisher.
- [5] Lastname, F. M., Alpha, B. G., Last, F. M., & Sunday, M. T. (2003). How to Write Bibliography. City: Publisher Company.
- [6] Physics, M., Bio, P., Medicine, P., Engineering, B., & Computational, S. (2013). On the Importance of Interdisciplinary Harmony. *Journal of Interdisciplinary Article Writing*, 5634-5650.
- [7] Ruby, S. T., & Oxygen, H. A. (2012). Scientific Writing in the Next Century: Will We Still Be Relevant? 17th Congress on Scientific Writing (pp. 39-43). City: Publishedby.

HOW TO SUBMIT IN JOURNAL OF MEDICAL PHYSICS AND BIOPHYSICS: AN AUTHOR'S TECHNICAL GUIDELINE

Prepared by Journal Manager

Journal of Medical Physics and Biophysics

E-mail: editor@jmpb.org

Abstract: This set is prepared to guide authors in going through the online procedure to submit their works in Journal of Medical Physics and Biophysics. Open Journal Systems are applied in JMPB procedures and the step-by-step procedures for submitting articles are described in this document. Authors may also see OJS's userguide for more illustrations.

Received Revised Accepted Published

Keywords: Author, paper, submit

I. Overview

OJS exists to serve Authors as well as journals. Not only does OJS provide an easy-to-use submission process, it can collect and disseminate key information about Authors and their work across important research and citation databases, including Google Scholar, PubMed, the Directory of Open Access Journals, and others.

As an Author, your tasks include submission; submitting revised copy; copyediting; and proofreading. To make a submission, you must have a user account and be enrolled as an Author. User accounts can be created by registering yourself. Once you have an account, log in to the journal site and select the role of Author.



Figure 1. Selecting the Author's role

II. The Author User Home Page

After clicking on the <u>Author</u> link on your User Home page, you will be directed to your Author's User Home page, which includes information on <u>Active Submissions</u>; a link to <u>start a new submission</u>; and information on any <u>Refbacks</u> you may have.

A. Active Submissions

This page will list any of your submissions to the journal that are still in process (e.g., awaiting assignment to an editor, undergoing review, being edited) or incomplete (in which case you can return and finish the submission at any point).

Each completed submission will fall into one of the following categories:

- Awaiting Assignment: the submission has been completed by you; you cannot now delete the submission from the system yourself. The Editor can now see the submission, and must assign an Editor or Section Editor to it.
- Queued for Review: the submission has been vetted and is now in the review process. You should receive notice shortly on the review decision.
- Queued for Editing: the submission has completed the review process and has been accepted for publication; it will now make its way through the system's copyediting, layout editing and proofreading processes.

In the example below, the journal is charging a submission fee to authors, and you must pay this (using the <u>Pay Submission Fee</u> link) before the submission can be considered. If a journal does not charge submission fees, this link would not appear. Similarly, this example journal is also configured to require a publication fee. The author must use the <u>Pay to Publish</u> link to make the payment and allow for publication to proceed. JMPB does not charge any fee for any process, so authors will not see these steps.

As the author, you can click on the hyperlinked title of any listed submission and review it. Clicking a submission title will bring you to your submission's Summary page. From here, you could revise the title or abstract (by clicking the Edit Metadata link). If the editor asks for revisions, you will upload the changes this way too (in the Review section of your submission).

B. RefBacks

The RefBacks section displays any incoming links from external web sites such as blogs, news sites, or other articles that link directly to your articles. Each RefBack can be edited: it can be ignored, deleted, or published, in which case it appears publicly at the end of your published article on the web site.

C. Archive

Your Archive page will list all declined submissions, as well as any published submissions along with information on which issue they appear in.



Figure 2. Active Submissions



Figure 3. Submission Summary

III. Submitting an Article

To make a submission, select the <u>Click Here</u> link (under Start a New Submission) to proceed to the <u>first step</u> of the submission process.

Start a New Submission
CLICK HERE to go to step one of the five-step submission process.

Figure 4. Starting a Submission

A. Submission Step One: Starting the Submission

Step 1 ensures that the Author understands the journal's submission rules. The Author will have to pick the appropriate section to submit to, and will be provided with information on the journal's privacy statement, copyright notice, competing interest statement and/or author fees, if applicable. If you need any help the journal's technical support contact is provided at the top of this page.

- First, if the journal charges <u>submission fees</u>, these will be presented to the author. If the journal does not charge submission fees, this section will not appear. This is not the case for JMPB.
- Next, the author must check each of the items from the submission checklist.
- The journal's copyright policy will appear next, and, if configured as a requirement, the author will need to agree to this policy.
- Finally, the author can add any comments, which will be visible to the editor. Move to the next step by hitting the <u>Save and Continue</u> button.

B. Submission Step Two: Uploading the Submission

Submission Step Two allows you to upload the submission file, typically a word-processing document.

- Click <u>Browse</u> to open a Choose File window for locating the file on the hard drive of your computer.
- Locate the file you wish to submit and highlight it.
- Click <u>Open</u> on the Choose File window, which places the name of the file on this page.
- Click <u>Upload</u> on this page, which uploads the file from the computer to the journal's web site and renames it following the journal's conventions.
- Once the submission is uploaded, click <u>Save and</u> continue.

C. Submission Step Three: Entering the Submission's Metadata

The third step of the submission process serves to collect all relevant metadata from the author. The first section of metadata covers the authors. The submitting author will have their personal information automatically appear. Any additional information, such as Competing Interests should also be added at this time, if required.

If there are multiple authors for the submission, their information can be added using the Add Author button. You can also re-order the list of authors, make one of the authors the principal contact with the editor, and delete any authors added in error. Next, enter the submission title and abstract. You will then add indexing information. This will help others find your article. The final section allows you to enter the name of any organization that may have supported your research.

Hit the <u>Save and Continue</u> button to move on to Step 4.

D. Submission Step Four: Uploading Supplementary Files

This step is optional. If you have any supplementary files, such as research instruments, data sets, etc., you may add them here. These files are also indexed by the author, identifying their relation to the submission, as well as their ownership. Supplementary Files can be uploaded in any file format and will be made available to readers in their original format

- Locate the file you wish to submit and highlight it.
- Click Open on the Choose File window, which places the name of the file on this page.
- Click <u>Upload</u> on this page, which uploads the file from the computer to the journal's web site and renames it following the journal's conventions.
- Once the submission is uploaded, click <u>Save and Continue</u>.

E. Submission Step Five: Confirming the Submission

This final step provides a summary of your submission. Click <u>Finish Submission</u> to submit your manuscript. You will receive an acknowledgement by email and will be able to view your submission's progress through the review and editorial process by returning to the <u>Active Submissions</u> section of your Author page.

F. Authors and Submission Review and Editing Process

To track your submission's progress through the review and editorial process, you will need to log into the journal web site, and choose your role as Author. Click on the linked title to go to the submission record.

CTI	MM-DD	HIVE			
ID	SUBMIT	SEC	AUTHORS	TITLE	STATUS
1	12-28	ART	Chan	A STUDY OF ELECTRONIC PUBLISHING	Awaiting assignment PAY SUBMISSION FEE
2	12-28	ART	Chan	LEARNING TO PUBLISH	IN REVIEW PAY SUBMISSION FEE
5	12-28	ART	Chan, MacIntosh	LIBRARIES AND PUBLISHING: NEW OPTIONS FOR RESEARCH	Awaiting assignment PAY SUBMISSION FEE
3	12-28	ART	Chan	OPEN SOURCE SOFTWARE AND SCHOLARLY PUBLISHING	IN EDITING PAY TO PUBLISH

Figure 5. Active Submissions

1. Summary

The Summary section contains several sections, including Submission, which displays the author names,

submission title, original submission file, any supplementary files, the ability to add a supplementary file, the name of the submitter, the date submitted, the section the article is assigned to, the editor responsible for the submission, and the comments to editor you made as part of your submission (see above).

From the resulting 'Summary' page, you will see links to <u>Summary</u>, <u>Review</u>, and <u>Editing</u> pages. Each of these pages will provide details about your submission.

The Status section lets you know where your submission is in the publishing process (see above for status possibilities). It also lets you know when you made your submission and the date of the most recent status change.

The final section outlines the submission metadata, including author details, title, abstract, indexing, and supporting agency. You can modify any of this information by selecting Edit Metadata.

2. Review

If your submission is In Review, you can view its details in the <u>Review</u> section (linked from the top of your page). First, you will see the basic submission information again. Below that is the Peer Review section. You will see information about each round of review (there may be one or more) and any revised files (e.g., a version of your original submission file with changes marked in) uploaded by each reviewer (Reviewer A, Reviewer B, etc.).

Last on this page is the Editor Decision section. From this section you can notify the editor once you have submitted your revised submission file, view the reviewer comments (click on the cloud icon), and upload your revised submission file (if revisions were required).

Possible decisions include:

- Accept: Your submission has been accepted as is.
- Revisions Required: Your submission requires minor changes and will be accepted once those have been completed.
- Resubmit for Review: Your submission needs significant re-working. A new file must be submitted and another round of review will take place.
- Reject: Your submission was not accepted for publication with this journal, either because it was not seen to be of high enough quality, or its subject did not match the journal.

3. Editing

Your submission is considered "In Editing" once it has been approved for publication. It will then need to go through copyediting to correct any grammatical or stylistic errors, layout editing to create the published galleys (e.g., HTML or PDF), and proofreading to take one final look at the article before it is made publicly available.

If your submission is In Editing, you can view its details in the <u>Editing</u> section (linked from the top of your page). The first section again includes basic submission information.

In the next section, you can follow the copyediting process.

 Step 1: The journal's Copyeditor has made changes to the reviewed submission file. You can download a revised copy here (e.g., 6-11-1-ED.DOCX).

- Step 2: You will review the Copyeditor'ss changes, and make any final changes of your own. You then upload your revised submission file here. Be sure to use the email icon to notify the Copyeditor that you have submitted your file.
- Step 3: The Copyeditor takes a last look at your changes before passing the submission over to the Layout Editor. No action is required by the author.

The next stage in the editorial process is layout editing. The Layout Editor takes the final copyedited version of the submission and converts it into a format suitable for publishing on the journal web site (e.g., typically HTML or PDF). These are known as the "galleys".

The final editing stage is proofreading. It is also broken down into 3 steps;

- Once the galleys have been uploaded by the Layout Editor, you will receive an email from the editor asking that you review them and note any errors in the Proofreading Corrections comments. Proofing Instructions are also available. To view these, you will need to login to the journal and select the appropriate submission link. On the resulting screen, you can use the View Proof links to display the files. You can click the linked file names (e.g, 1-95-1-PB.HTML) to download a copy. Review the files and make comments any using the Layout Comments icon. Once you have completed your review and noted any necessary changes, hit the Complete button. This will generate an email informing the Proofreader and Section Editor that you are satisfied with the galleys.
- The journal's own Proofreader will also check for errors and make their own notes and inform the Layout Editor when all proofreading is complete. No action is required by the Author.
- The Layout Editor takes all of the notes and incorporates all of the changes into revised galleys.

These are then ready to publish. No action is required by the Author.

You have now completed all of the steps involved in submitting to the journal and participating in the review and editing of your submission.

IV. ACKNOWLEDGMENTS

JMPB refers this complete guide from OJS instructions. We are thankful for the systems provided by OJS.

REFERENCES

- [1] Open Journal Systems user guide
- [2] International Reference Writing Agency. (2004). *How to Write Reference List Properly*. Cityname: References Press.
- [3] JMPB Editor. (2013). How to Publish in Journal of Medical Physics and Biophysics: An Author's General Guideline. *J. Med. Phys. Biop.*, *I*(1), 1-3.
- [4] Lastname, F. M. (2000). Book Title. City: Publisher.
- [5] Lastname, F. M. (2011). Putting References with the Right Manner. In F. M. January, & Q. J. King, *Writing an Article May Not Be Difficult* (pp. 234-270). Cityname: Publisher.
- [6] Lastname, F. M., Alpha, B. G., Last, F. M., & Sunday, M. T. (2003). *How to Write Bibliography*. City: Publisher Company.
- [7] Physics, M., Bio, P., Medicine, P., Engineering, B., & Computational, S. (2013). On the Importance of Interdisciplinary Harmony. *Journal of Interdisciplinary Article Writing*, 5634-5650.
- [8] Ruby, S. T., & Oxygen, H. A. (2012). Scientific Writing in the Next Century: Will We Still Be Relevant? *17th Congress on Scientific Writing* (pp. 39-43). City: Publishedby.

HOW TO REVIEW ARTICLES IN JOURNAL OF MEDICAL PHYSICS AND BIOPHYSICS: A REVIEWER'S GUIDELINE

Prepared by Journal Manager

Journal of Medical Physics and Biophysics

E-mail: editor@jmpb.org

Abstract: This set is prepared to guide reviewers in going through the online procedure to review submitted works in Journal of Medical Physics and Biophysics. Open Journal Systems are applied in JMPB procedures and the step-by-step procedures for reviewing articles are described in this document. Reviewers may also see OJS's userguide for more illustrations.

Received Revised Accepted Published

Keywords: Article, paper, review

I. Overview

The Reviewer is invited by email to review a submission, which includes its title and abstract, as well as the journal's URL and a username and password for the Reviewer to use to enter the journal. The journal has the option of using a reviewer option that sends the submission as an email attachment to the Reviewer along with an invitation to review.

In this case, the Reviewer then responds by email via a provided link. What is described here is the principal method for reviewing (and ensuring complete records of the process), which involves the Reviewer conducting the Review on the journal's web site.

II. Review Home Page

A. Submissions

On logging in to the journal, you will arrive at the User Home page.



Figure 1. Reviewer Home

To see the submissions you need to review, click the Reviewer link, or click the "x" Active link. Both will take you to your active Submissions page. This page lists the submissions which you have been invited to review or are currently in the process of reviewing.

The Submissions queue also notes what round the review is, as some reviews may have entered a second round of reviewing, following the Section Editor's decision that the submission must be "resubmitted for review." This page also provides access to past reviews which the Reviewer has completed for the journal.

Clicking on the linked title will take you to the review process.

B. Review

You will first see a summary of the submission details.



Figure 2. Review Assignment

Next, you will see the review schedule, and the associated deadline. Next, the Review process is divided into seven steps.

- You have first to indicate to the Section Editor whether they will undertake the review. The decision should be made after reviewing the submission's Abstract and perhaps looking at the submission, by clicking on the file name in Step 3 (depending on the journal's policies, the file may not be available before agreeing to review it).
- If you are unable to do the review, click on <u>Unable to</u> do the review which leads to a standard email to the Section Editor.
- If able to do the review, click on <u>Will do the review</u>, which leads to a standard email to the Section Editor, and which will indicate to Section Editor and Author that the review is underway.
- Consult the <u>Reviewer Guidelines</u>, found at the bottom of the Review page. The Reviewer Guidelines have been prepared by the Editors of the journal to ensure that your review is as helpful as possible to them and the author.
- The Author has uploaded the submission as a file, which you can download from the journal's web site to your computer by clicking on the file name. The Supplementary Files refer to materials the Author may have uploaded in addition to the submission, such as data sets, research instruments, or source texts.

- (Optional): In some cases, the journal may require you to declare whether or not you have competing interests with the article being reviewed. If this is the case, this step becomes a form requesting a declaration of Competing Interests, and all following steps change their step number accordingly.
- Click on the Review icon and is presented with two Review text-boxes where the Review can be either entered by hand or pasted: one for the Editor and Author, and one visible to the Editor only. The Reviewer may enter or paste partial reviews into these boxes and click the <u>Save</u> button at the bottom of the form to return and make changes later. The Reviewer may return to make such changes until a recommendation on the main Review pages is chosen, at which time the Review process is complete.
- Please note: the Journal manager, in conjunction with the journal's Editor(s), may have created an extended custom review form to be filled out here. More information on the custom form should be found in the Reviewer's Guidelines. The form can be returned to and edited until a recommendation has been chosen
- You also have the option, in addition to entering a review, of uploading files for the Section Editor and/or the Author to see. These files may be an annotated version of the submission or some relevant data or other materials that will assist Editor and/or Author. It will be at the Editor's discretion whether these files are shown to the Author, but you can certainly comment on this in the Review (Step 5).
- You must select a Recommendation for the submission from among the following options: Accept, Revisions Required, Resubmit for Review, Resubmit Elsewhere, Decline Submission, See

Comments. When you click <u>Submit Review to the Editor</u>, it leads to a prepared email to the Section Editor, and makes your recommendation, saved Review (which is now locked) and any uploaded files available to the Editor.

III. ACKNOWLEDGMENTS

JMPB refers this complete guide from OJS instructions. We are thankful for the systems provided by OJS.

REFERENCES

- [1] Open Journal Systems user guide
- [2] International Reference Writing Agency. (2004). *How to Write Reference List Properly*. Cityname: References Press.
- [3] JMPB Editor. (2013). How to Publish in Journal of Medical Physics and Biophysics: An Author's General Guideline. *J. Med. Phys. Biop.*, *I*(1), 1-3.
- [4] Lastname, F. M. (2000). Book Title. City: Publisher.
- [5] Lastname, F. M. (2011). Putting References with the Right Manner. In F. M. January, & Q. J. King, Writing an Article May Not Be Difficult (pp. 234-270). Cityname: Publisher.
- [6] Lastname, F. M., Alpha, B. G., Last, F. M., & Sunday, M. T. (2003). *How to Write Bibliography*. City: Publisher Company.
- [7] Physics, M., Bio, P., Medicine, P., Engineering, B., & Computational, S. (2013). On the Importance of Interdisciplinary Harmony. *Journal of Interdisciplinary Article Writing*, 5634-5650.
- [8] Ruby, S. T., & Oxygen, H. A. (2012). Scientific Writing in the Next Century: Will We Still Be Relevant? *17th Congress on Scientific Writing* (pp. 39-43). City: Publishedby.

ACTIVITY CALENDAR 2014

University of Indonesia

Training on Dosimetry for Diagnostic Radiology

Held collaboratively with BPFK Jakarta Venue: UI Depok Campus

AAPM-UI-RSCM Modern Clinical Radiotherapy Workshop

http://medphys.fisika.ui.ac.id

Lectures and practical sessions by AAPM experts Venue: Cipto Mangunkusumo Hospital

Workshop on Medical Image Processing

One week practical sessions and one week research updates by Prof. Wolfgang Birkfellner (Medical University of Vienna, Austria) Venue: UI Depok Campus March 13-15

August 27-30

September 7-21

Workshop on Interventional Radiology

November/ December

Lecture by Prof. Hilde Bosmans (KU Leuven, Belgium) Venue: to be announced 13 14 15 20 21 28

> Department of Physics, Faculty of Mathematics and Natural Sciences, University of Indonesia UI Depok Campus, 16424, INDONESIA +62 21 7872610, +62 21 7863441 (Fax)





JOURNAL MEDICAL PHYSICS AND BIOPHYSICS

CALL FOR PAPERS

The Journal of Medical Physics and Biophysics cordially invites papers to be published on the second issue due published on August 2014. Online submission for publication consideration can be performed at any time before May 31st 2014.

The journal is the official publication media of Indonesian Association of Medical Physics and Biophysics and is authorized by:

EDITORS

Chief Supriyanto Ardjo Pawiro, Ph.D

Deputy Yessie Widya Sari, M.Si

BOARD OF REVIEWERS

Chief Djarwani S. Soejoko, Prof. Dr. University of Indonesia

Members Kin Yin Cheung, Ph.D IOMP

Wahyu Setia Budi, Prof. Dr.

Diponegoro University

H. J. Freisleben, Prof. Dr. rer. med. habil. University of Indonesia

James C. L. Lee, Ph.D NCC Singapore

Musaddiq Musbach, Dr. rer. nat.

University of Indonesia

Hye-Kyung Son, Ph.D KFDA South Korea Johan Noor, Ph.D Brawijaya University

Husin Alatas, Dr. Bogor Agricultural University
Idam Arif, Dr. Bandung Institute of Technology

Gede Bayu Suparta, Ph.D Gadjah Mada University

Freddy Haryanto, Dr. rer. nat. Bandung Institute of Technology

PUBLISHER CONTACT

Email: editor@jmpb.org

Medical Physics and Biophysics Division, Department of Physics, Faculty of Mathematics and Natural Sciences, University of Indonesia, Depok, 16424, West Java, INDONESIA

Print ISSN: 2355-2727 | Online ISSN: 2355-2719 | http://jmpb.org



JOURNAL OF MEDICAL PHYSICS AND BIOPHYSICS

Secretariat and Publisher:

Medical Physics and Biophysics Division, Department of Physics, Faculty of Mathematics and Natural Sciences, University of Indonesia Depok, 16424, INDONESIA

http://www.jmpb.org | editor@jmpb.org

JMPB is the official publication media of: Indonesian Association of Medical Physics and Biophysics (HFMBI)

